Surrogate models for seismic response analysis of flexible rocking structures

Originally published in:
Earthquake Engineering & Structural Dynamics, https://doi.org/10.1002/eqe.4193

Funding acknowledgement:
184805 - Quasi-Dynamic Seismic Performance-Based Design Procedure (SNF)

Received: 6 December 2023 | Revised: 24 June 2024 | Accepted: 25 June 2024

DOI: 10.1002/eqe.4193

RESEARCH ARTICLE

WILEY

Surrogate models for seismic response analysis of flexible rocking structures

Andréia Horta Alvares da Silva | **Božidar Stojadinović**

Institute of Structural Engineering, Department of Civil, Environmental and Geomatic Engineering, ETH Zurich, Zurich, Switzerland

Correspondence
Andréia Horta Alvares da Silva, Chair of Structural Dynamics and Earthquake Engineering, Institute of Structural Engineering, Department of Civil, Environmental and Geomatic Engineering, ETH Zürich, Zurich 8092, Switzerland.
Email: a.alvaresdasilva@ibk.baug.ethz.ch

Funding information
Schweizerischer Nationalfonds zur Förderung der Wissenschaftlichen Forschung, Grant/Award Number: 200021_184805; ETH Zurich

Abstract

Seismic design tools are based on surrogate models of the designed structure and the responses of those surrogates to earthquake ground motions. To design symmetric flexible rocking structures, a surrogate model that includes rocking and flexure is needed. In this paper, we derive the equation of motion of a flexible multi-degree-of-freedom (MDOF) structure rocking on its base in modal coordinates. Then, we introduce a set of two-degree-of-freedom (2DOF) surrogate models that accounts only for the first elastic vibration mode of the multimass structure and its rotation about the base pivot points. We investigate the surrogates' ability to represent the dynamics of an elastic MDOF structure that uplifts and rocks and the interaction between rocking and flexure. Therein, we detail the simplifications for the equations of motion of the 2DOF surrogate models and the adopted rocking impact model, and develop and check the sliding initiation condition. We show that the simplified 2DOF surrogate model responses compare well to experimental results. Then we assess the 2DOF surrogate model accuracy in representing the earthquake response of the MDOF model using Cloud Analysis and the coefficient of determination R^2 approach. We find that simplified 2DOF surrogate of the MDOF model is quite accurate ($R^2 = 0.99$) in estimating its maximum relative top displacement and acceptably accurate ($R^2 = 0.90$) in estimating its maximum base rotation based on a thousand randomly generated flexible rocking structure earthquake response analyses. Lastly, we discuss using the simplified 2DOF surrogate model of symmetric flexible rocking structures in preliminary seismic design, and give examples featuring a continuous elastic hollow semi-conical chimney and an inelastic flexible MDOF structure, both with a base that may uplift.

KEYWORDS
flexure, rocking, sliding, surrogate model, uplift

1 | INTRODUCTION

When a structure uplifts and rocks on its base, its base shear force and overturning moment are limited by its weight through its rocking-resisting moment. Housner[1] investigated this seismic protection feature, inspired by the observation that some tall slender structures were hardly damaged during the 1960 Valdivia (Chile) earthquake due to their ability to uplift and rock, compared to severely damaged fixed-base structures. Rocking structures, however, are not new: they were built by the Egyptians, Minoans, Greeks, and Chinese as early as several thousand years ago.[2]

Lately, rocking isolation has been adopted in different building and bridge designs. Pioneering rocking structures in New Zealand include a reinforced concrete rocking chimney,[3] the Rangitikei river bridge with rocking piers,[4] and the Wigram–Magdala Link Bridge with dissipative rocking-controlled devices.[5] Enhanced dynamic behavior of buildings can be achieved with rocking wall,[6–8] rocking frame,[9,10] and rocking podium[11–13] systems. Zhong and Christopoulos[2] present an extensive review of research on and different applications of rocking as a seismic isolation technique.

An important element of a seismic design procedure is a surrogate model of the designed, prototype structure. The responses of a surrogate model to suites of earthquake ground motions are used to derive the earthquake response spectra and various seismic response prediction equations[14–18] used for design. Today, a single-degree-of-freedom (SDOF) surrogate model is at the center of most seismic design procedures. Nevertheless, a SDOF surrogate model has limits, particularly as it can not represent complex behavior transitions and interactions, such as that between rocking and flexure.[19]

In this paper, we present a two-degree-of-freedom (2DOF) surrogate model capable of representing the seismic response of flexible structures that may uplift and rock on their base, including transitions and interactions between flexure and rocking response modes. This 2DOF surrogate model is intended to be the basis of a seismic design procedure that addresses modern applications of rocking isolation for flexible structures.

While there is a remarkable body of work addressing the rocking motion of rigid bodies (e.g., 1, 20–22 to name a few), only some papers have addressed the seismic behavior of flexible rocking structures. In 1975, Meek[23] investigated the dynamic response of a single-mass flexible structure rocking on a rigid foundation. A few years later, Psycharis[24] investigated structures with a single-mass and with multiple masses rocking on a two-spring or on a Winkler foundation, and Yim and Chopra[25,26] developed a simplified method for analyzing such structures. More recently, Oliveto et al.[27] derived the equations of motion of a flexible structure allowed to uplift subjected to large rotations; Vassiliou et al.[28] investigated the behavior of a flexible cantilever with distributed and concentrated masses rocking on a rigid base; Acikgoz and DeJong[29] also investigated the behavior of a flexible system with multiple degrees of freedom rocking on a rigid base.

In our work, we first integrate the previous achievements in modeling the dynamics of multimass flexible rocking structures to standardize the notation following Chopra.[30] From the work of Yim and Chopra[25,26] and Psycharis,[24] we adopt the transformation from Cartesian to modal coordinates. From Acikgoz and DeJong,[29] we adopt the Lagrangian derivation of the equation of motion that includes the centrifugal and Coriolis forces in the formulation. We adopt and simplify the impact model of Vassiliou et al.,[28] and formulate the equation of motion of a flexible multi-degree-of-freedom (MDOF) structure that can uplift and rock on a rigid base in modal coordinates. Then, we introduce graduated simplifications of this equation of motion to formulate a series of 2DOF surrogate models and introduce a constraint against sliding during rocking. Next, we compare the earthquake responses of the 2DOF surrogate models to that of the (MDOF) model to investigate the surrogate accuracy. We find that the simplified 2DOF surrogate model is able to represent the statistics of the seismic response quantities of interest of the MDOF model. Thus, it can be used in preliminary seismic design procedures as it has reduced number of input parameters and entails a lesser response computing effort. To facilitate using the simplest 2DOF surrogate model in preliminary seismic design procedure for flexible rocking structures, we compute its parameters for different elastic or inelastic symmetric multimass prototype structures. Further, we illustrate the use of this model to compute the response of a flexible rocking semi-conical chimney structure to an earthquake ground motion. Finally, we adapt the simplified 2DOF surrogate model to consider the inelastic behavior of flexible rocking structure using a Bouc-Wen hysteresis model.

2 | THE ROCKING-FLEXURE PROBLEM

Herein, we focus on a general flexible structure with vertically distributed lumped masses on top of a rigid base that can uplift and rock or a rigid foundation surface. Such a multi-degree-of-freedom (MDOF) structure typically represents

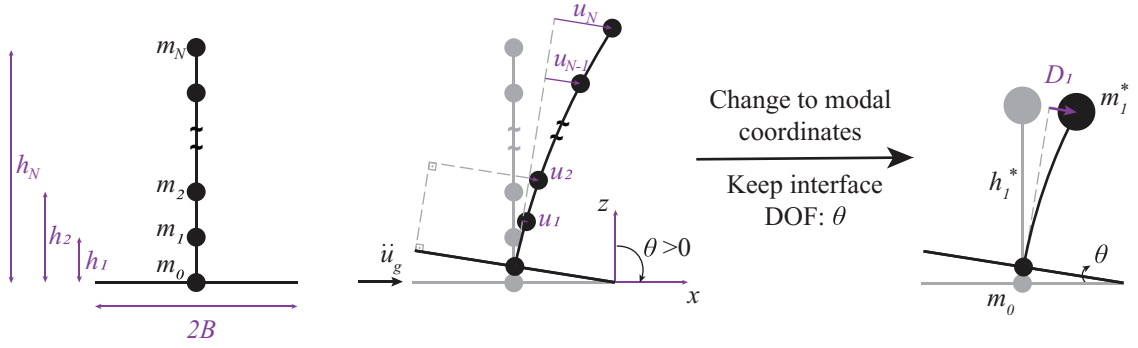

FIGURE 1 On the left-hand side, the geometry and the degrees of freedom of the MDOF structure with a rigid base rocking on a rigid foundation. The translation degrees of freedom of the N MDOF structure masses u_i are parallel to the base of the structure and relative to the base mass. The angle of uplifted base rotation about a pivot point θ is the remaining degree of freedom. On the right-hand side, the modal analysis procedure to transform a MDOF rocking structure into a 2DOF surrogate model.

multistory buildings, bridge columns, towers, chimneys, and so forth. The MDOF structure has N lumped masses m_i, assembled into a structural mass matrix $\boldsymbol{m_s}$. It rests on a rigid base with a lumped mass m_0 that may uplift and rock, as shown in Figure 1. Each of the structural masses is associated with a displacement u_i degree of freedom, assembled into a structural displacement vector $\boldsymbol{u}_s$, while the base mass m_0 is associated only with the rotation degree of freedom, θ, of the base about the pivot point. Displacements of the MDOF structure masses u_i are relative to the rigid base and remain parallel to it as it uplifts (Figure 1). The vertical distances between the masses of the structure m_i and the base mass m_0 are given by the vector of heights $\boldsymbol{\iota_h} = [h_1\ h_2\ \ldots\ h_N]^T$, while the width of the rigid base is $2B$. The idealized structure behaves elastically in flexure: its stiffness is defined by the stiffness matrix $\boldsymbol{k_s}$ relative to the displacement u_i of the masses. We use the superposition of modal damping (Equation 11.4.21 in Chopra [30]) to obtain the damping matrix $\boldsymbol{c_s}$ of the MDOF structures, implying that every mode has the same damping ratio ζ. This damping model is widely adopted[31] and allows to assign the same damping ratio for all modes considered. The MDOF structure is excited by a horizontal ground motion $\ddot{u}_g$ and moves in-plane. We assume that the base of the MDOF structure does not slide to derive the equations of motion, but we provide an equation to check if sliding occurred.

2.1 | Complete model of the MDOF rocking structure

The equations of motion of a MDOF structure on top of a rocking base have been already developed.[24,25,29] The work of Acikgoz and DeJong[29] presents the complete formulation that accounts for the Centrifugal and Coriolis forces. To their work, we add one more step: the transformation from the Cartesian coordinates to the modal coordinates. This step is also not new as other authors[24,25] already applied it to the linearized version of the equations of motion. Lastly, Vassiliou et al.[28] derived the equation of motion for a flexible column with a concentrated mass on top using its modal properties. In their work, they also account for the Centrifugal and Coriolis forces. Herein, we integrate these findings to formulate the equation of motion of a MDOF structure on a rigid massive rocking base in modal coordinates as follows.

When there is no base uplift, the equations of motion of the MDOF structure are:

$$\boldsymbol{m_s}\ddot{\boldsymbol{u}}_s + \boldsymbol{c_s}\dot{\boldsymbol{u}}_s + \boldsymbol{k_s}\boldsymbol{u}_s = -\boldsymbol{m_s}\boldsymbol{\iota}\ddot{u}_g\,, \tag{1}$$

where $\boldsymbol{\iota}$ is a column vector of ones. The uplift condition is: the absolute value of the overturning moment M_o must be greater than the resisting moment M_r, that is:

$$\mp M_o = \mp\left(\boldsymbol{\iota_h^T}\boldsymbol{m_s}(\ddot{\boldsymbol{u}}_s + \boldsymbol{\iota}\ddot{u}_g)\right) > \left(\boldsymbol{\iota}^T\boldsymbol{m_s}(B \mp \boldsymbol{u_s}) + m_0 B\right)g = \mp M_r\,. \tag{2}$$

If the overturning moment is negative, the base uplifts and the MDOF structure rotates around the right pivot point of the base ($\theta > 0$, the upper sign in Equation 2); conversely, if M_o is positive, the MDOF structure rotates around the left pivot point ($\theta < 0$, the lower sign in Equation 2). We use this sign convention throughout this paper.

The coordinates of the MDOF structure masses after uplift, in a Cartesian coordinate system centered on the pivot points, are defined by the vector:[28]

$$r_i = \begin{bmatrix} r_{i,x} \\ r_{i,z} \end{bmatrix} = \begin{bmatrix} \mp B\cos\theta + h_i \sin\theta + u_i \cos\theta \\ \pm B\sin\theta + h_i \cos\theta - u_i \sin\theta \end{bmatrix}. \tag{3}$$

We perform a modal analysis ($\boldsymbol{k_s\Phi} = \boldsymbol{m_s\Phi\Omega^2}$) to find the undamped vibration modes of the MDOF structure and convert the translations $\boldsymbol{u_s}$ of the MDOF structure masses to the modal coordinates $u_i = \sum_{n=1}^{N} q_n\phi_{i,n}$. The coordinates q_n are the modal coordinates, ω_n are the modal vibration frequencies $\boldsymbol{\Omega}^2 = diag(\omega_n^2)$ and $\boldsymbol{\phi_n}$ are the vibration mode shape vectors of the MDOF structure $\boldsymbol{\Phi} = [\phi_1\ ,\phi_2\ ,\ \ldots\ ,\phi_n]$. To represent the coordinates of the base mass, we add a line of zeros to $\boldsymbol{\Phi}$, thus $\phi_{0,n} = 0$ for any n, as the vibration mode shapes of the MDOF structure are defined relative to the base mass. Then, the coordinates of all masses with respect to the pivot point are:

$$r_i = \begin{bmatrix} \mp B\cos\theta + h_i \sin\theta + \cos\theta \sum_{n=1}^{N} q_n\phi_{i,n} \\ \pm B\sin\theta + h_i \cos\theta - \sin\theta \sum_{n=1}^{N} q_n\phi_{i,n} \end{bmatrix}, \tag{4}$$

where i identifies the mass and ranges from 0 to N.

The derivative of the mass coordinates with respect to time is:

$$\dot{r}_i = \begin{bmatrix} \pm B\dot{\theta}\sin\theta + h_i\dot{\theta}\cos\theta + \cos\theta \sum_{n=1}^{N} \dot{q}_n\phi_{i,n} - \dot{\theta}\sin\theta \sum_{n=1}^{N} q_n\phi_{i,n} \\ \pm B\dot{\theta}\cos\theta - h_i\dot{\theta}\sin\theta - \sin\theta \sum_{n=1}^{N} \dot{q}_n\phi_{i,n} - \dot{\theta}\cos\theta \sum_{n=1}^{N} q_n\phi_{i,n} \end{bmatrix}. \tag{5}$$

The kinetic energy of the MDOF structure and its rigid massive base is:

$$E_k = \sum_{i=0}^{N} \frac{1}{2} m_i \|\dot{r}_i\|^2 = \sum_{i=0}^{N} \frac{1}{2} m_i \left(\dot{\theta}^2 \left(B^2 + h_i^2 \mp 2B \sum_{n=1}^{N} \phi_{i,n} q_n + \sum_{n=1}^{N} \phi_{i,n}^2 q_n^2 \right) + 2h_i\dot{\theta} \sum_{n=1}^{N} \phi_{i,n}\dot{q}_n + \sum_{n=1}^{N} \phi_{i,n}^2 \dot{q}_n^2 \right). \tag{6}$$

The potential energy of the MDOF structure and its rigid massive base is:

$$E_p = \sum_{i=0}^{N} m_i g r_{i,z} + \sum_{i=0}^{N} m_i \ddot{u}_g r_{i,x} + \int_0^u F_s du\,, \tag{7}$$

where $F_s = \boldsymbol{k_s u_s}$ represent the static resistance forces of the MDOF structure. Therefore:

$$E_p = \sum_{i=0}^{N} m_i g \left(\pm B\sin\theta + h_i\cos\theta - \sin\theta \sum_{n=1}^{N} q_n\phi_{i,n} \right) + \sum_{i=0}^{N} m_i \ddot{u}_g \left(\mp B\cos\theta + h_i\sin\theta + \cos\theta \sum_{n=1}^{N} q_n\phi_{i,n} \right) + \frac{\mathbf{q^T\Phi^T k_s \Phi q}}{2}, \tag{8}$$

in which the last term becomes a summation given the orthogonality between $\boldsymbol{\Phi}$ and $\boldsymbol{k_s}$. Specifically: $\mathbf{q^T\Phi^T k_s \Phi q} = \sum_{n=1}^{N} q_n^2\omega_n^2 \left(\sum_{i=1}^{N} m_i\phi_{i,n}^2 \right)$.

We apply the Lagrangian ($L = E_k - E_p$) to the degrees of freedom of the massive rigid base and the MDOF structure θ and q_n, respectively. For θ:

$$\frac{\partial L}{\partial \theta} - \frac{\mathrm{d}}{\mathrm{d}t}\left(\frac{\partial L}{\partial \dot{\theta}} \right) = 0\,. \tag{9}$$

For q_n, we adopt the *Rayleigh dissipation function*[32,33] to include the energy dissipated by nonconservative forces in the MDOF structure (herein through viscous damping). Note that we use superposition of modal damping, not Rayleigh damping. In doing so, we profit from the orthogonality of the MDOF structure damping matrix with respect to the vibration mode shapes $\boldsymbol{\Phi}$. Thus, damping in each mode is $\boldsymbol{\phi_n^T c_s \phi_n} \dot{q}_n$. Using orthogonality of the MDOF structure mode shapes, modal damping can also be written as $\dot{q}_n 2\zeta\omega_n \sum_{i=1}^{N} m_i \phi_{i,n}^2$ (Equation 11.4.16 in Chopra [30]). Therefore, the Lagrangian for q_n with structural damping is:

$$\frac{\partial L}{\partial q_n} - \frac{\mathrm{d}}{\mathrm{d}t}\left(\frac{\partial L}{\partial \dot{q}_n}\right) + \dot{q}_n 2\zeta\omega_n \sum_{i=1}^{N} m_i \phi_{i,n}^2 = 0\,. \tag{10}$$

We rewrite Equation (9) to obtain the equation of motion for θ that describes the moment equilibrium around the pivot point:

$$\begin{aligned} &-\sum_{i=0}^{N} m_i g\left(\pm B\cos\theta - h_i\sin\theta - \cos\theta\sum_{n=1}^{N} q_n\phi_{i,n}\right) - \sum_{i=0}^{N} m_i\ddot{u}_g\left(\pm B\sin\theta + h_i\cos\theta - \sin\theta\sum_{n=1}^{N} q_n\phi_{i,n}\right) \\ &-\sum_{i=0}^{N} m_i\left(\ddot{\theta}(B^2+h_i^2) \mp \ddot{\theta}2B\sum_{n=1}^{N}\phi_{i,n}q_n \mp \dot{\theta}2B\sum_{n=1}^{N}\phi_{i,n}\dot{q}_n + \ddot{\theta}\sum_{n=1}^{N}\phi_{i,n}^2 q_n^2 + \dot{\theta}\sum_{n=1}^{N}2\phi_{i,n}^2\dot{q}_n q_n + h_i\sum_{n=1}^{N}\phi_{i,n}\ddot{q}_n\right) = 0\,. \end{aligned} \tag{11}$$

Moreover, Equation (10) becomes a set of N equations in terms of modal degrees of freedom q_n:

$$\begin{aligned} &\mp\sum_{i=0}^{N} m_i\dot{\theta}^2 B\phi_{i,n} + \sum_{i=0}^{N} m_i\dot{\theta}^2\phi_{i,n}^2 q_n + \sum_{i=0}^{N} m_i g\sin\theta\phi_{i,n} - \sum_{i=0}^{N} m_i\ddot{u}_g\cos\theta\phi_{i,n} \\ &-q_n\omega_n^2\left(\sum_{i=1}^{N} m_i\phi_{i,n}^2\right) - \sum_{i=0}^{N} m_i h_i\ddot{\theta}\phi_{i,n} - \sum_{i=0}^{N} m_i\phi_{i,n}^2\ddot{q}_n - \dot{q}_n 2\zeta\omega_n\sum_{i=1}^{N} m_i\phi_{i,n}^2 = 0\,. \end{aligned} \tag{12}$$

We adopt the notation defined in Chopra[30] for the MDOF structure: $L_n^h = \sum_{i=1}^{N} m_i\phi_{i,n}$, $L_n^\theta = \sum_{i=1}^{N} h_i m_i\phi_{i,n}$, $M_n = \sum_{i=1}^{N} m_i\phi_{i,n}^2$, $\Gamma_n = L_n^h/M_n$, $m_n^* = \Gamma_n L_n^h$, and $h_n^* = L_n^\theta/L_n^h$. Additionally, for convenience, we scale the modal coordinate $q_n = \Gamma_n D_n$ with respect to the displacement of the equivalent modal SDOF system D_n using the modal participation factor Γ_n. Consequently, Equation (11) becomes:

$$\begin{aligned} I_\theta\ddot{\theta} \pm m_{tot}gB\cos\theta - L_0^r g\sin\theta \pm m_{tot}\ddot{u}_g B\sin\theta + L_0^r\ddot{u}_g\cos\theta + \sum_{n=1}^{N}\Big(&\mp\ddot{\theta}2Bm_n^* D_n + \ddot{\theta}m_n^* D_n^2 + m_n^* h_n^*\ddot{D}_n \\ &+2\dot{\theta}\dot{D}_n m_n^*(\mp B + D_n) - g\cos\theta m_n^* D_n - \ddot{u}_g\sin\theta m_n^* D_n\Big) = 0\,, \end{aligned} \tag{13}$$

where $I_\theta = \sum_{i=0}^{N} m_i(h_i^2 + B^2)$, $m_{tot} = \sum_{i=0}^{N} m_i$ and $L_0^r = \sum_{i=0}^{N} m_i h_i$. Similarly, the N equations contained in Equation (12) become:

$$h_n^*\ddot{\theta} + \ddot{D}_n + 2\zeta\omega_n\dot{D}_n + \omega_n^2 D_n - g\sin\theta + \dot{\theta}^2(\pm B - D_n) = -\ddot{u}_g\cos\theta\,, \tag{14}$$

for the degrees of freedom D_n of each mode.

Lastly, for completeness, the equations of motion of the MDOF structure before uplift are:[30]

$$\ddot{D}_n + 2\zeta\omega_n\dot{D}_n + \omega_n^2 D_n = -\ddot{u}_g\,, \tag{15}$$

one for each mode degree of freedom. The condition for rocking initiation (RI) is:

$$\mp\left(\sum_{n=1}^{N} m_n^* h_n^*\ddot{D}_n + L_0^r\ddot{u}_g\right) > m_{tot}gB \mp \sum_{n=1}^{N} m_n^* g D_n\,. \tag{16}$$

2.1.1 | Impact model

The classical impact model for rigid-rocking blocks assumes instantaneous impact, conservation of angular momentum, and concentration of the impact forces at the pivot point.[1] This model is not adequate for flexible structures; therefore, Meek,[23] Acikgoz and DeJong,[34] and others developed alternative models. Vassiliou et al.[28] analyzed the coherence of different impact models by comparing experimentally obtained pulse and earthquake excitation response of a single-mass rigid rocking structure to those obtained using different analytical models. Following their work, we adopt the Vertical Velocity Energy Loss (VVEL) model, also adopted by others.[23,25,35] In the VVEL model, the collision between the base and the foundation is perfectly inelastic without bouncing; thus, the vertical velocity is completely dissipated, implying $\dot{\theta}$ is equal to zero and the structure sticks to the ground after impact. Also, in the VVEL model, the horizontal kinetic energy of the masses is conserved; therefore, the horizontal kinetic energy before $E_{hk,b}$ and the total kinetic energy after impact $E_{k,a}$ are equal (which is a model assumption and not a physical law). The horizontal kinetic energy before impact is:

$$E_{hk,b} = \sum_{i=1}^{N} \frac{1}{2} m_i (h_i \dot{\theta}_b + \dot{u}_{i,b})^2 = \frac{1}{2} \left[\dot{\theta}_b^2 \left(\sum_{i=1}^{N} m_i h_i^2 \right) + 2\dot{\theta}_b \sum_{n=1}^{N} m_n^* h_n^* \dot{D}_{n,b} + \sum_{n=1}^{N} m_n^* \dot{D}_{n,b}^2 \right], \tag{17}$$

The total kinetic energy after impact is:

$$E_{k,a} = \sum_{i=1}^{N} \frac{1}{2} m_i \dot{u}_{i,a}^2 = \frac{1}{2} \sum_{n=1}^{N} m_n^* \dot{D}_{n,a}^2 . \tag{18}$$

Thus, we equate $E_{hk,a}$ and $E_{k,b}$ to obtain the impact model:

$$\sum_{n=1}^{N} m_n^* \dot{D}_{n,a}^2 = \dot{\theta}_b^2 \left(\sum_{i=1}^{N} m_i h_i^2 \right) + 2\dot{\theta}_b \sum_{n=1}^{N} m_n^* h_n^* \dot{D}_{n,b} + \sum_{n=1}^{N} m_n^* \dot{D}_{n,b}^2 . \tag{19}$$

Note that the sign of the velocity before impact must be separately accounted for in Equation (19) to calculate the post-impact velocity because squaring these quantities obscures their sign. Moreover, this equation has no solution, as only one such equation is available for N unknown velocities $\dot{D}_{n,a}$ after the impact. Other approaches are possible. For example, if one adopts a local impact model (as in, for example, in a finite element simulation), it is possible to solve for the post-impact velocities of the MDOF model masses. We adopt the VVEL impact model given its good agreement with experimental results[36] and its simplicity, but other models can also be used. For example, the impact model introduced by Giouvanidis and Dimitrakopoulos[37] covers all physically feasible post-impact states, such as bouncing or repeated uplifting. Another example is the impact model for flexible structures proposed by Zhu et al.[38] based on a series of momentum equations. The impact models presented above were developed for rocking structures with uniform mass and elastic stiffness distributions. Thus, they need to be modified to represent structures with multiple non-uniformly distributed masses and stiffness.

2.1.2 | Sliding initiation

Throughout the presented derivations, we assume that the base of the MDOF rocking structure does not slide on its rigid foundation. Yet, we need to check the validity of this assumption. Sliding initiates when the sum of the horizontal forces in the MDOF rocking structure exceeds the friction resistance. Using a simple static friction model, the friction resistance is equal to the total self-weight of the MDOF rocking structure multiplied by the fiction coefficient μ_f:

$$\left| \sum F_x \right| > \left| \mu_f \sum F_z \right| . \tag{20}$$

The sum of horizontal forces is:

$$\sum F_x = \sum_{i=0}^{N} m_i \left(\ddot{u}_g + \ddot{\theta}(\pm B \sin\theta + h_i \cos\theta - u_i \sin\theta) + \ddot{u}_i \cos\theta + \dot{\theta}^2(\pm B \cos\theta - h_i \sin\theta - u_i \cos\theta) - 2\dot{\theta}\dot{u}_i \sin\theta \right), \tag{21}$$

and the sum of vertical forces is:

$$\sum F_z = \sum_{i=0}^{N} m_i\Big(-g + \ddot{\theta}(\pm B\cos\theta - h_i\sin\theta - u_i\cos\theta) - \ddot{u}_i\sin\theta + \dot{\theta}^2(\mp B\sin\theta - h_i\cos\theta + u_i\sin\theta) - 2\dot{\theta}\dot{u}_i\cos\theta\Big). \quad (22)$$

2.2 | Simplified model of the MDOF rocking structure

To simplify the equations of motion of a MDOF rocking structure, we assume that the base uplift angle θ is small, making $\sin\theta = \theta$, $\cos\theta = 1$, that the Centrifugal and Coriolis forces are too small compared to the other forces, and that the displacements of the MDOF structure masses are small compared to the size of its base, that is, $B - u_i \approx B$. Therefore, the equations of motion (Equations 13 and 14) become:

$$\begin{bmatrix} I_\theta & (diag(\boldsymbol{m}^*)\boldsymbol{h}^*)^T \\ \boldsymbol{h}^* & \mathbf{1} \end{bmatrix} \begin{bmatrix} \ddot{\theta} \\ \ddot{\boldsymbol{D}} \end{bmatrix} + \begin{bmatrix} 0 & \mathbf{0} \\ \mathbf{0} & diag(2\zeta\omega_n) \end{bmatrix} \begin{bmatrix} \dot{\theta} \\ \dot{\boldsymbol{D}} \end{bmatrix} + \begin{bmatrix} -L_0^r g & \mathbf{0} \\ \mathbf{0} & diag(\omega_n^2) \end{bmatrix} \begin{bmatrix} \theta \\ \boldsymbol{D} \end{bmatrix} \pm \begin{bmatrix} m_{tot} gB \\ \mathbf{0} \end{bmatrix} = - \begin{bmatrix} L_0^r \\ \mathbf{1} \end{bmatrix} \ddot{u}_g \,. \quad (23)$$

Similarly, Equation (16), that defines RI in the MDOF rocking structure, becomes:

$$\left| \sum_{i=1}^{N} m_i^* h_i^* \ddot{D}_i + L_0^r \ddot{u}_g \right| > m_{tot} gB \,. \quad (24)$$

Importantly, we also simplify the impact model, by assuming that each mass has its horizontal kinetic energy conserved, that is $\dot{\boldsymbol{u}}_{\boldsymbol{s,a}} = \dot{\boldsymbol{u}}_{\boldsymbol{s,b}} + \boldsymbol{\iota_h}\dot{\theta}_b$, thus:

$$\dot{\boldsymbol{D}}_{\boldsymbol{a}} = \boldsymbol{h}^*\dot{\theta}_b + \dot{\boldsymbol{D}}_{\boldsymbol{b}} \,. \quad (25)$$

Note that Equation (25) is a set of N equations for N unknowns $\dot{D}_{n,a}$, making a solution possible as opposed to Equation (19) that has no solution.

2.3 | 2DOF surrogate models of the MDOF rocking structure

We apply the substructure method (also known as component mode synthesis[39,40]) to create a 2DOF surrogate model of a flexible prototype MDOF rocking structure (Figure 1). The method consists of dividing the structure into sub-structures and interface degrees of freedom. Each sub-structure is reduced in complexity by exchanging the current DOFs by a few modal coordinates that are obtained with modal analysis considering the interface DOFs fixed. Herein the application is simple: the interface degree of freedom is the base rotation angle θ while the sub-structure is the MDOF system with masses m_1 to m_n. We exchange all the coordinates u_i with the first mode modal coordinates D_1 to obtain the two degrees of freedom (2DOF) surrogate model.

Then, the equation of motion for the DOF θ of the 2DOF surrogate model (derived from Equation 13) is:

$$\begin{aligned} I_\theta\ddot{\theta} \mp \ddot{\theta}2Bm_1^*D_1 + \ddot{\theta}m_1^*D_1^2 + m_1^*h_1^*\ddot{D}_1 + 2\dot{\theta}\dot{D}_1m_1^*(\mp B + D_1) + g(\pm m_{tot}B\cos\theta - L_0^r\sin\theta - m_1^*\cos\theta D_1) \\ = -\ddot{u}_g\left(\pm m_{tot}B\sin\theta + L_0^r\cos\theta - m_1^*\sin\theta D_1\right). \end{aligned} \quad (26)$$

Similarly, the equation of motion for the DOF D_1 of the 2DOF surrogate model (derived from Equation 14) is:

$$h_1^*\ddot{\theta} + \ddot{D}_1 + 2\zeta\omega_1\dot{D}_1 + \omega_1^2D_1 - g\sin\theta + \dot{\theta}^2(\pm B - D_1) = -\ddot{u}_g\cos\theta \,. \quad (27)$$

The condition to initiate rocking for the 2DOF surrogate model is:

$$\mp\left(m_1^*h_1^*\ddot{D}_1 + L_0^r\ddot{u}_g\right) > m_{tot}gB \mp m_1^*gD_1 \,, \quad (28)$$

and the impact model of the 2DOF surrogate model is:

$$m_1^* \dot{D}_{1,a}^2 = \dot{\theta}_b^2 \left(\sum m_i h_i^2 \right) + 2 m_1^* h_1^* \dot{\theta}_b \dot{D}_{1,b} + m_1^* \dot{D}_{1,b}^2 \,. \tag{29}$$

To obtain the simplified versions of the 2DOF surrogate model we assume that the angle θ is small, making $\sin\theta = \theta$ and $\cos\theta = 1$, that the Centrifugal and Coriolis forces are too small compared to the other forces, and that the displacements of the MDOF structure masses are small compared to the size of its base, that is, $B - u_i \approx B$. Therefore, the simplified equations of motion of the 2DOF surrogate model are:

$$\begin{bmatrix} I_\theta & m_1^* h_1^* \\ h_1^* & 1 \end{bmatrix} \begin{bmatrix} \ddot{\theta} \\ \ddot{D}_1 \end{bmatrix} + \begin{bmatrix} 0 & 0 \\ 0 & 2\zeta\omega_1 \end{bmatrix} \begin{bmatrix} \dot{\theta} \\ \dot{D}_1 \end{bmatrix} + \begin{bmatrix} -L_0^r g & 0 \\ 0 & \omega_1^2 \end{bmatrix} \begin{bmatrix} \theta \\ D_1 \end{bmatrix} \pm \begin{bmatrix} m_{tot} g B \\ 0 \end{bmatrix} = - \begin{bmatrix} L_0^r \\ 1 \end{bmatrix} \ddot{u}_g \,, \tag{30}$$

where $L_0^r = \sum_{i=0}^{N} m_i h_i$, and m_1^*, h_1^* and ω_1 are the modal properties of the first mode (Section 2.1).

The simplified condition to initiate rocking of the 2DOF surrogate model is:

$$\left| m_1^* h_1^* \ddot{D}_1 + L_0^r \ddot{u}_g \right| > m_{tot} g B \,, \tag{31}$$

and the simplified impact model is:

$$\dot{D}_{1,a} = h_1^* \dot{\theta}_b + \dot{D}_{1,b} \,. \tag{32}$$

3 | COMPARISON OF MDOF ROCKING STRUCTURE MODELS

In the previous section, we present five different models of a MDOF structure rocking on a rigid foundation, summarized in Figure 2. Equations (13) and (14) of the complete MDOF rocking structure model are complex to solve, and the impact model that we chose (Equation 19) has no solution for systems with more than two degrees of freedom, making this complete MDOF model impractical for us. Therefore, we derive the equations for four models, as shown in (Figure 2): (i) the complete 2DOF surrogate model 2DOF-C based on Equations (26), (27), (28), and (29); (ii) the 2DOF surrogate model with simplified impact model 2DOF-C-SI based on Equations (26), (27), (28), and (32); (iii) the 2DOF surrogate simplified model 2DOF-S based on Equations (30), (31), and (32); and (iv) the MDOF rocking structure simplified model MDOF-S based on Equations (23), (24), and (25). To simulate the response of each of these models to base excitation, we implement the associated equations in MATLAB [41] and created separate model solver routines based on the MATLAB *ode15s* differential equation solver.

In the following, we first compare the implemented models with respect to their ability to reproduce experimentally obtained response history of prototypes MDOF rocking structures. Then, we use the MDOF-S and 2DOF-S models to probabilistically evaluate the rocking angle and relative top displacement response quantities of the prototype MDOF rocking structure. Finally, we address the effect of higher vibration modes on estimating the said response quantities and indicate how to extend the 2DOF-S surrogate model to include a few higher vibration mode shapes.

3.1 | Time history model response comparison to experimental results

The first experiment results we compare our surrogate models to are obtained from Truniger et al.,[36] while the second experiment is that of Acikgoz and DeJong [29]. Truniger et al.[36] experiments involved a flexible cantilever column with a weight on top, mounted on a rigid baseplate that can uplift and rock. The column was placed on a rigid shaking table surface and excited by various excitation time histories. In this paper, we focus on specimen 2Hz-Long Base(14) subjected to an antisymmetric Ricker pulse motion with peak acceleration $a_p = 0.1g$ and period $T_p = 0.5s$.

Four models of specimen 2Hz-Long Base(14), 2DOF-C, 2DOF-C-SI, 2DOF-S, and MDOF-S, were instantiated using the specimen properties reported in Truniger et al.[36] We develop a finite element model of the fixed-base specimen (similar to the application example in Section 4.1.1) for the calculation of the modal and rocking properties m_n^*, h_n^*, I_θ, L_0^r, and $m_{tot} g B$.

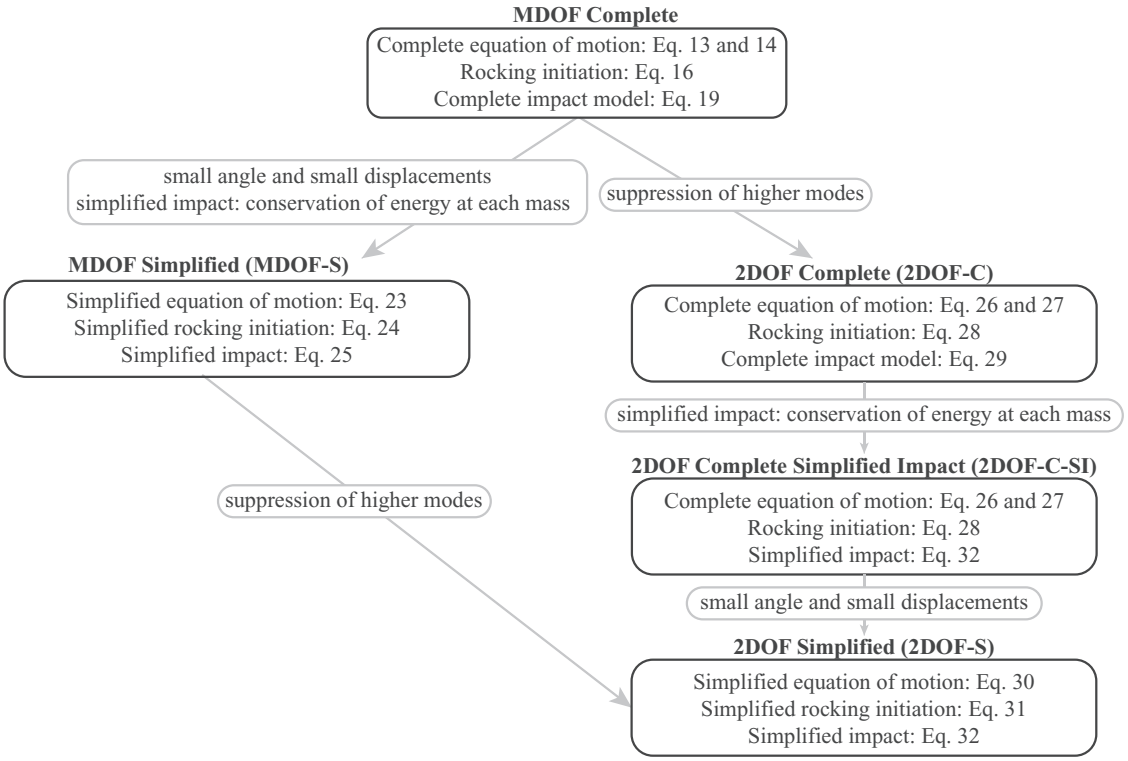

FIGURE 2 Different MDOF rocking structure models and 2DOF surrogate models. 2DOF, two-degree-of-freedom; MDOF, multi-degree-of-freedom.

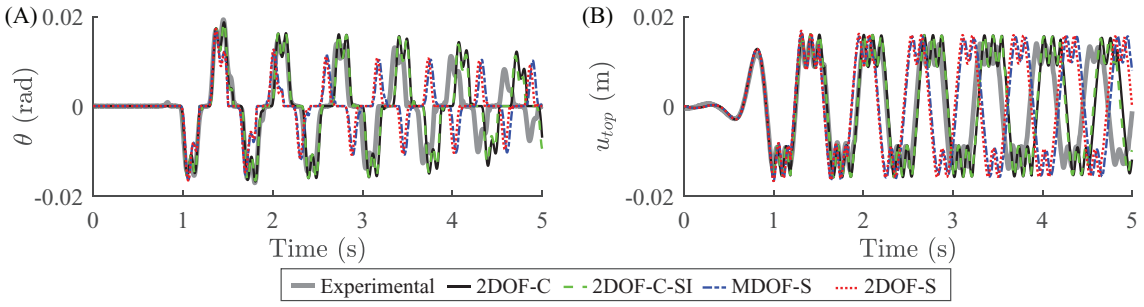

FIGURE 3 Comparison of the rotation (panel A) and relative top displacement (panel B) responses obtained from shaking table test of specimen 2Hz-Long-Base(14)[36] under the anti-symmetric Ricker pulse excitation (continuous gray thick line) to those obtained using the 2DOF-C (continuous black line), 2DOF-C-SI (dashed green line), MDOF-S (dashed blue line) and 2DOF-S (dotted red line) models.

To build the MDOF-S model, we use only the first two vibration modes, while we use only the first vibration mode of the fixed-base specimen to build both 2DOF models. The resulting rotation and relative top displacement time-history graphs are shown in Figure 3 for the four models and compared to the experiment outcomes.

The responses of the complete 2DOF-C and 2DOF-C-SI models are very similar to those obtained from the 2Hz-Long Base(14) experiment, particularly over the first few rocking cycles. The simplified models MDOF-S and 2DOF-S are very similar to each other. Even though both simplified models reproduce the peaks of the specimen responses, they match the experiment data only in the first two response cycles. The simplified models have shorter rocking periods and seem to dissipate more energy than the specimen. Two factors may contribute to the shorter rocking cycles: the energy dissipated in the impact model discussed in Section 2.1.1, and the difference in the resisting moment of the simplified model and the complete model. The resisting moment of the complete 2DOF-C model is $M_r = \pm m_{tot} gB\cos(\theta) - m_1^* D_1 g\cos(\theta) - L_0^r g\sin(\theta)$, while the resisting moment of the simplified model 2DOF-S is $M_r = \pm m_{tot} gB - L_0^r g\theta$. The resisting moment of the simplified model is approximately 7% larger, causing the model to return the column base into contact with the

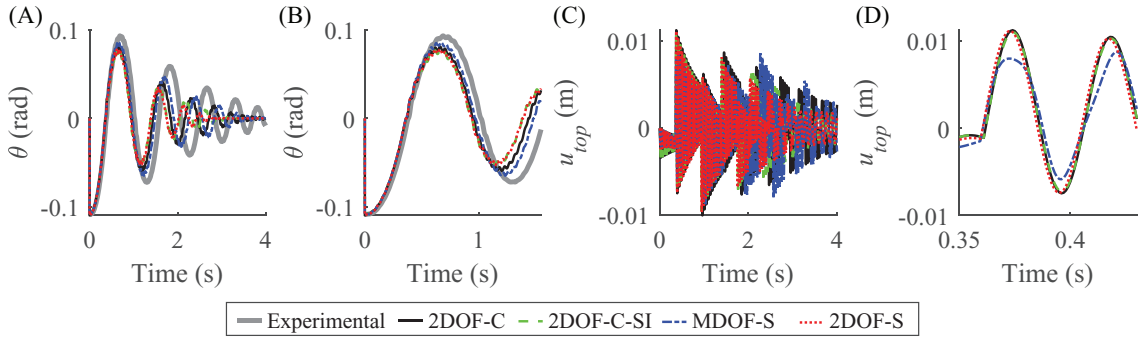

FIGURE 4 Comparison of the rotation (panels A and B) and relative top displacement (panels C and D) responses obtained with our models and the rotation of specimen S1[29] during a free vibration test with initial rotation angle $\theta_{ini} = 0.11$ rad.

ground faster. Yet, if only the maximum responses are of interest, any of the four models can be used to estimate them with sufficient accuracy.

Specimen 2Hz-Long-Base can be represented well by a 2DOF surrogate model: its base overturning (OV) moment first-mode modal participation factor is $m_1^* h_1^* / L_0^r = 0.98$ and its base shear first-mode modal participation factor is $m_1^*/m_{s,tot} = 0.92$, where $m_{s,tot} = \sum_{i=1}^{N} m_i$. To contrast, we created four models (MDOF-S, 2DOF-S, 2DOF-C, 2DOF-C-SI) of specimen S1 from Acikgoz and DeJong[29] and compared our analysis results with the results of their specimen S1 free vibration test from which we only had access to rotation θ data. This specimen is a steel column welded to a stiff steel plate mounted on four steel feet. The column has five different irregularly spaced masses attached to it along its height. We highlight the modal participation factors $m_1^* h_1^* / L_0^r = 0.87$ and $m_1^*/m_{s,tot} = 0.48$ of specimen S1 to stress that a 2DOF surrogate models may not represent the response this specimen well. We ran our four models for the free vibration test with an initial rotation angle $\theta_{ini} = 0.11$ rad, and plot the resulting time histories of rotation and relative top displacement in Figure 4.

All four models agree well with the rotation angle θ of the specimen for the first rocking cycle (Figure 4B). However, at every impact, models' rotations increasingly deviate from the recorded rotation angles (Figure 4B). One reason is that specimen S1 rotates almost immediately around the other pivot point after the impact occurs, while our impact model forces the structure to stick to the ground before initiating the next rocking cycle. Another important difference between specimens S1 and 2Hz-Long-Base is in their first-mode natural periods: 0.11 s for specimen S1 model (the reported experimentally obtained value is 0.13 s) and 0.5 s of specimen 2Hz-Long-Base model. Even though the relative top displacement test results were not available to us, we plot the time history of this response quantity for the four models in Figure 4C,D. In contrast to the models of specimen 2Hz-Long-Base, for specimen S1 the relative top displacement of the MDOF-S model is about 21% smaller than those produced by the 2DOF models, indicating the effect of higher vibration modes. Notably, models 2DOF-C, 2DOF-S, and 2DOF-C-SI give almost identical relative top displacements.

Truniger et al.[36] observed some sliding of the flexible cantilever specimens even when they covered the top surface of the shaking table with sandpaper to increase its friction coefficient. A flexible cantilever oscillator will start rocking if the inverse of its aspect ratio B/h_1^* is smaller than the friction coefficient μ_f, as shown in Section 2.1.2. Otherwise, it will slide. Yet, even if the oscillator begins to rock, it may still slide. The spike in the specimen motion at the beginning of each rocking cycle can explain this observation. During such a spike, the total horizontal force developed at the base of the specimen can be larger than that needed to trigger rocking: therefore, sliding may occur even if $B/h_1^* < \mu_f$. Nevertheless, the duration of this spike is very short: if sliding occurs, we expect that sliding displacements will be small. Moreover, Acikgoz et al.[42] also observed sliding (around 4 mm) in their experiment with specimen S1, particularly during impact, which confirms the observation of the analytical models: the response spikes in the beginning of a rocking cycle may cause some sliding.

We use the responses obtained using the complete model 2DOF-C of specimen 2Hz-Long-Base(14) (Figure 3) to check for sliding. We compute the ratio of the sum of horizontal forces (Equation 21) divided by the sum of the vertical forces (Equation 22). The smallest calculated force ratio is 0.27; it is larger than the inverse of the specimen aspect ratio $B/h_1^* = 0.16$. Given that the friction coefficient of the sandpaper placed on the shaking table surface was larger than 0.27, we would not expect the specimen to slide. Yet, small sliding displacements, on the order of 0.3 mm, were observed during specimen 2Hz-Long-Base(14) tests.[36] We believe such displacements are small enough to be attributed to the imperfections of the sandpaper surface.

TABLE 1 Parameters of the six 5-story prototype rocking structures.

#	T_1	h_1^*/B	ρ	$I_\theta/(m_1^* h_1^{*2})$	$(m_1^* h_1^*)/L_0^r$	$m_n^*/(5m_i)$	h_n^*/h_5
1	1	10	∞	1.03	1.03	[0.88 0.09 0.02 0.008 0.002]	[0.70 −0.24 0.15 −0.12 0.10]
2	1	10	0	1.05	0.90	[0.68 0.21 0.07 0.03 0.01]	[0.79 0.23 0.14 0.10 0.09]
3	0.5	10	∞	1.03	1.03	[0.88 0.09 0.02 0.008 0.002]	[0.70 −0.24 0.15 −0.12 0.10]
4	0.5	10	0	1.05	0.90	[0.68 0.21 0.07 0.03 0.01]	[0.79 0.23 0.14 0.10 0.09]
5	1	5	∞	1.07	1.03	[0.88 0.09 0.02 0.008 0.002]	[0.70 −0.24 0.15 −0.12 0.10]
6	1	5	0	1.10	0.90	[0.68 0.21 0.07 0.03 0.01]	[0.79 0.23 0.14 0.10 0.09]

When performing the same analysis with the MDOF-S model results obtained for specimen S1, we conclude that this specimen should have been sliding after impact for any reasonable friction coefficient value (i.e., the force ratios in Equation 20 were higher than 2). We traced the occurrence of such large minimum friction coefficients to a shortcoming of our impact model: it cannot always accurately predict the structure's rotation acceleration $\ddot{\theta}$. When the structure finishes a rocking cycle and almost immediately starts a new rocking cycle around the other pivot point, rotation acceleration $\ddot{\theta}$ computed by the impact model spikes. This is a consequence of the impact model assumption that the structure sticks to the ground after impact, forcing the rotation velocity $\dot{\theta}$ to zero. When the next rocking cycle starts around the other pivot point, the structure rapidly regains angular velocity $\dot{\theta}$ resulting in a spike of the rotation acceleration $\ddot{\theta}$ values. Consequently, the values of the sum of the vertical forces F_z calculated with Equation (22) also spike, precluding a correct calculation of the minimum friction coefficient necessary for the structure not to slide.

3.2 | Accuracy of the simplified models for probabilistic response estimation

We compare the seismic responses of the MDOF-S, 2DOF-S, and 2DOF-C models to assess the differences between the statistics of the responses of the 2DOF-S, 2DOF-C, and MDOF-S models. Given that the solution of the differential equations of equilibrium and impact of the complete MDOF-C model is impractical for us due to our impact model choice, we adopt the MDOF-S model to compute the benchmark response of the prototype MDOF rocking structure. In this process, we assume that base rotation θ and angular velocity $\dot{\theta}$ as well mass displacements u_i of the MDOF rocking structure are small, as is the case for rocking structures that are far from OV, a desired situation from the design standpoint. The principal difference between the MDOF-S and 2DOF-S models is the number of degrees of freedom above the rocking base. Thus, the 2DOF-S surrogate model cannot capture the effects that the higher vibration modes of the prototype MDOF rocking structure may have on its maximum responses to recorded ground motions.

For this comparison, we form a family of six prototype rocking structures, detailed in Table 1. Each structure is a five-story single-bay frame, with uniform story stiffness and floor mass distribution along the height. The height of each story is $L_c = 3$ m, thus $h_i = i \times 3$ m. The base of each structure can uplift. It has a mass m_0 equal to the mass of a story $m_i = 40$ ton and a length equal to $2B$. The modal damping ratio for each fixed-base vibration mode is set to 2%, a standard assumption for this type of structure. We do not analyze other damping ratios herein. Acikgoz and DeJong[34] analyzed the influence of the damping ratio on the stability of the flexible rocking structure, finding that more damped structures are more prone to OV. Nevertheless, the difference is slight for damping ratio values between 0.5% and 10% damping.

The behavior of three of the prototype MDOF rocking structures is shear-dominant, while the behavior of the remaining three is flexure-dominant. This behavior mode distinction is achieved by adjusting the beam stiffness to set the beam-to-column stiffness ratio $\rho = (\sum_{beams} EI_b/L_b)/(\sum_{columns} EI_c/L_c)$ to ∞ or 0, respectively, following the derivation in Chopra.[30] The beam-to-column stiffness ratio dictates the modal properties of the prototype rocking structures listed in Table 1: they are independent of the vibration periods. The first vibration mode period T_1 of the prototype rocking structures is set to either 1.0 or 0.5 s by adjusting their column stiffness. The aspect ratio of the prototype rocking structures h_1^*/B is set to 5 or 10 by adjusting the value of the base length $2B$ with respect to the modal height h_1^*.

We perform Cloud Analysis to compute the statistics of the response of each prototype rocking structure (Table 1) using the MDOF-S, 2DOF-C, and the 2DOF-S models.[43] We use both horizontal components of the earthquake ground motions $\ddot{u}_g$ of a set of 105 firm-soil ordinary ground motion records (non-pulse, no-long-duration) that Regianni et al.[44] and Kazantzi et al.[18] previously adopted for analysis of rocking oscillators. To observe higher values of rocking angles, we

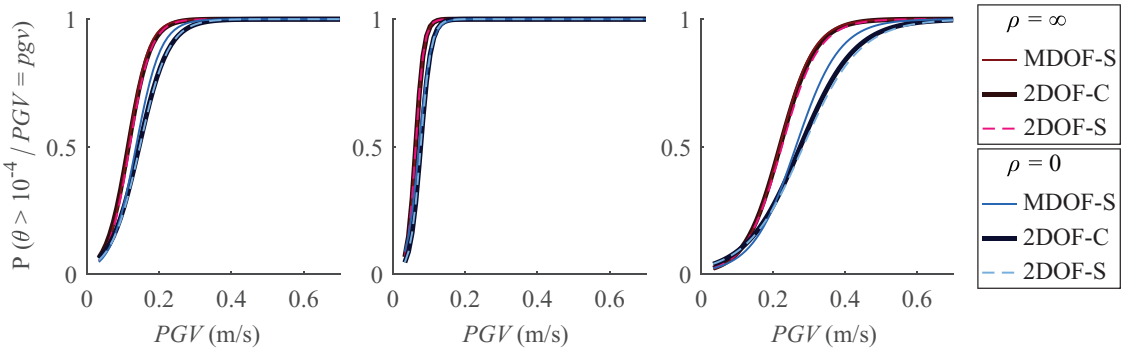

FIGURE 5 Fragility curves for RI conditioned on PGV obtained with logistic regression of the Cloud Analysis results. On the left, the fragilities for structures #1 and #2, in the middle, the fragilities for structures #3 and #4, and on the right, the fragilities for structures #5 and #6 of Table 1. The MDOF-S, 2DOF-C, and 2DOF-S models are differentiated by color and line type. RI, rocking initiated.

scale this record set by two and run the models again, totaling 420 analysis for each prototype structure listed in Table 1. We ran these analyses in MATLAB [41] on ETH Zürich's Euler parallel computer cluster, and used function *ode15s* to solve for their response time histories with a residual relative tolerance (*'RelTol'*) equal to 10^{-14}, the minimum practically possible. Then, we determine the absolute maxima of the response quantities of interest, which are the rocking angle θ_{max} and the relative top displacement $u_{top,max}$ for each ground motion analysis and its respective peak ground velocity (PGV). Note that $u_{top} = u_N$ (Figure 1) is relative to the model centerline perpendicular to the base and does not represent the absolute displacement of the top mass. The later is described by the change of position vector $\boldsymbol{r_i}$ (Equation 3), which accounts for the rigid body rotation of the base.

We separate each response data cloud into three groups depending on the outcome: no rocking initiation (NRI), RI, and OV. We start by analyzing if the three models (MDOF-S, 2DOF-C, and 2DOF-S) agree on the probability of significant rocking, defined as $P(\theta > 10^{-4}\text{rad})$. We chose the 10^{-4} rad threshold as it eliminates analysis where the effect of rocking on the time history of the relative top displacement is barely detectable). For this analysis, we choose the peak ground velocity *PGV* as the intensity measure because it has been shown to describe the behavior of rocking oscillators well.[18,45,46] We perform a logistic regression on the response data to obtain the fragility curves in Figure 5. The fragility curves produced by the three models agree well, with the largest differences occurring when comparing the MDOF-S to both 2DOF models for flexure-dominant ($\rho = 0$) structures. The reason for this discrepancy is the difference in the modal participation factors for the base-OV moment $m_1^* h_1^* / L_0^r$ (Table 1) of the models, given its role in RI (Equation 2).

The response data clouds of the RI group and the respective regression lines are shown in Figures 6 and 7 for the six different prototype structures and three different models, all as a function of the *PGV* earthquake intensity measure. We observe that, for the absolute maxima of the rotation angle θ_{max}, there is a good statistical agreement between the three models. For example, for a $PGV = 0.4$ m/s, the largest difference between the medians was 0.002 rad (15%) and between the 84% quantiles was 0.005 rad (12%). For absolute maxima of the relative top displacement $u_{top,max}$, the statistics of the 2DOF-C and 2DOF-S results agree well, but they differ from the statics of the MDOF-S model. For example, for a $PGV = 0.4$ m/s, the largest difference between the medians was 19% (0.003 m) and between the 84% quantiles was 22% (0.004 m); this difference is observable for building #3 in Figure 7. Interestingly, for the flexure-dominant structures ($\rho = 0$), the 2DOF models tend to underestimate the absolute maxima of the relative top displacement $u_{top,max}$ compared to the MDOF-S model. Conversely, for the shear-dominant structures ($\rho = \infty$), the 2DOF models tend to over-estimate the absolute maxima of the relative top displacement $u_{top,max}$ when compared to the MDOF-S model.

The comparisons between the MDOF-S, 2DOF-S, and 2DOF-C models herein rely on the same impact model. Modeling the impact of a rocking structure is still a challenge because the rocking response is very sensitive to initial conditions and contact surface imperfections. In this study we investigate the ability of 2DOF surrogate models to represent the response of MDOF flexible rocking structures that do not overturn. Using the same impact model for MDOF and 2DOF models facilitates this comparison, even if the adopted impact model is not as good in predicting OV as it is for simulating rocking without OV. The same comparisons could be performed using other impact models as discussed in Section 2.1.1. This effort was, however, not in the scope of our study.

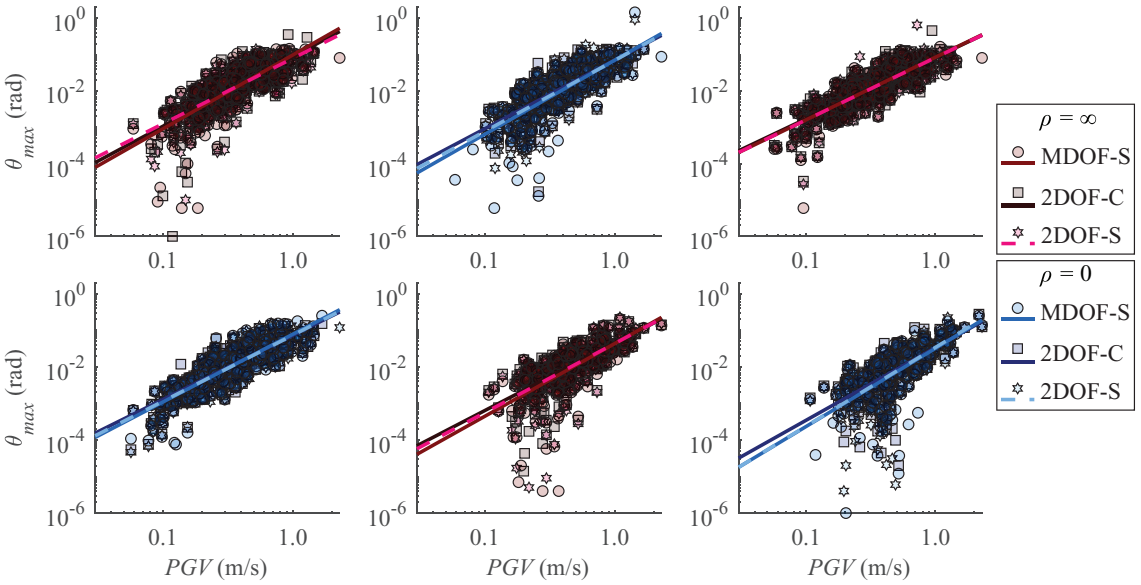

FIGURE 6 Clouds of response data from the 420 analyses of each prototype structure listed in Table 1 in cases when rocking has initiated and has not caused OV. The plotted points are the maximum absolute rotation angle θ_{max} and the PGV of each analysis. The structures are presented in order from top left to bottom right. The data points are differentiated by symbol and the regression lines $log(\theta_{max}) = c_1 + c_2 \log(PGV)$ for each model are differentiated by color and line type. OV, overturning.

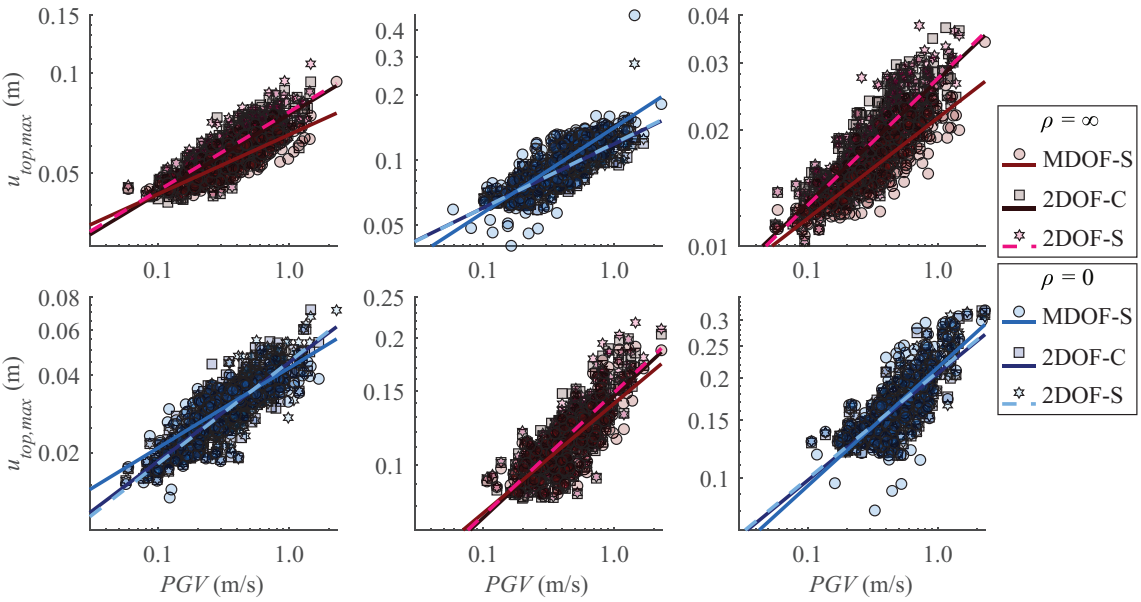

FIGURE 7 Cloud of response data from the 420 analyses of each prototype structure listed in Table 1 in cases when rocking has initiated and has not caused OV. The plotted points are the maximum absolute relative top displacement $u_{top,max}$ and the PGV of each analysis. The structures are presented in order from top left to bottom right. The data points are differentiated by symbol and the regression lines $log(u_{top,max}) = c_1 + c_2 \log(PGV)$ for each model are differentiated by color and line type. OV, overturning.

Lastly, we assume throughout this study that rocking occurs without sliding, supposing that the adequate mechanical sliding restraints[10,47–50] are provided or that the friction coefficient between the base and the foundation is large enough. For the Cloud Analysis response simulations presented in this section, we calculated the friction coefficient needed to prevent sliding using Equations (20), (21), and (22). We find that buildings with lower aspect ratios and shorter first-mode vibration periods are more prone to sliding. We also find that the shear-dominant buildings are more prone to sliding than the flexure-dominant ones. Nevertheless, there are cases where the minimum friction coefficient required to prevent

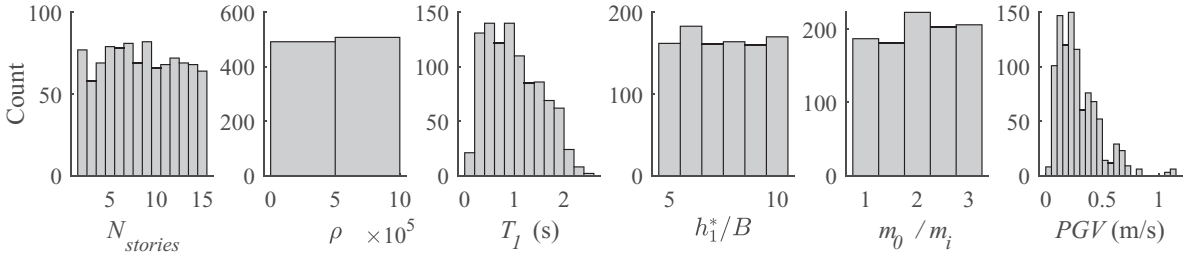

FIGURE 8 Distribution of the random prototype MDOF rocking structure characteristics and the PGV of the randomly selected ground motion.

sliding was higher than 1.0. As discussed above, such high friction coefficient values may be a consequence of the impact model and the rotation acceleration $\ddot{\theta}$ spikes it produces at the beginnings of rocking cycles.

3.3 | Accuracy of the 2DOF surrogate model for maximum ground motion response prediction

In the previous section, we compare the results of the MDOF-S, 2DOF-C, and 2DOF-S models for six different prototype five-story rocking structures using incremental dynamical analysis. In this section, we assess the accuracy of the 2DOF-S model to predict the MDOF-S model responses for a thousand different prototypes. First, a prototype rocking structure is randomly generated, and a ground motion is randomly selected. Then two time-history response analyses are run: one using the 2DOF-S and the other using the MDOF-S model solver.

The random prototype MDOF rocking structure is a single-bay multi-story frame structure with uniform story height $L_c = 3\,m$, uniform story mass $m_i = 40$ ton, and uniform story stiffness determined to attain a desired first vibration mode period value. The number of stories is a random integer uniformly distributed between 2 and 15. The aspect ratio of the structure is a random integer uniformly distributed between 5 and 10. The base mass is a multiple of the story mass, where that multiple is randomly selected from the set $\{1.0, 1.5, 2.0, 2.5, 3.0\}$. Each randomly generated prototype MDOF rocking structure is either shear-dominant ($\rho = \infty$) or flexure-dominant ($\rho = 0$), as explained in the previous section and in Chapter 19 of Chopra [30]. Finally, the story stiffness is adjusted to attain a random first-mode natural vibration period that varies according to two equations: for the shear-dominant structure $T = a_1 \cdot H^{0.85}$ with a random coefficient a_1 uniformly distributed in the $\{0.06, 0.095\}$ interval; and for the flexure-dominant structure $T = a_2 \cdot H$ with a random coefficient a_2 uniformly distributed in the $\{0.0125, 0.05\}$ interval. Note that the latter two equations are not the same as, but are based on the work of Chopra and Goel [51] to generate reasonable period values. The modal damping ratio of the generated prototype MDOF rocking structure is set to 2% in every one of its vibration modes.

The earthquake ground motion $\ddot{u}_g$ used to excite the prototype MDOF rocking structure models is randomly selected from the same earthquake set used in the previous section (210 firm-soil non-pulse, no-long-duration ground motion record components). The distributions of the generated prototype MDOF rocking structures characteristics are presented in Figure 8, together with the peak ground velocity PGV of the randomly selected motions. Using the MDOF-S and 2DOF-S model solvers, we determined the absolute maxima of the same response quantities as in the previous section.

The simulations are divided into three groups depending on the outcome: NRI, RI, and OV. The OV group contains a single simulation in which $\theta_{max} = \pi/2$ for the MDOF-S model. In this simulation, the two models do not completely agree: the 2DOF-S does not overturn, but the rocking angle is higher than $\tan^{-1}(B/h_1^*)$, practically indicating OV. If we use the nominal overturn threshold $\theta > 0.7\tan^{-1}(B/h_1^*)$ to indicate OV, 10 MDOF-S and six 2DOF-S cases overturn. However, we keep these analyses in the RI group to assess the accuracy of the 2DOF-S surrogate model for large θ values.

The NRI group contains the 306 simulations where the base rotation $\theta = 0$ for the MDOF-S model. Notably, rotation θ was not zero in only two 2DOF-S model simulations in the NRI group, but it was smaller than 5×10^{-5} indicating that the base of the 2DOF-S model was practically fixed. Thus, the two models agree well with respect to RI. A comparison between maximum absolute relative top displacements obtained using the MDOF-S and the 2DOF-S models in the NRI group is in Figure 9A. The agreement between the two models is very good, with a coefficient of determination $R^2 = 0.99$. Interestingly, the largest discrepancies between the two models occurred for prototype MDOF rocking structures with more than 10 stories (Figure 9A). The reason for such differences is that the response of fixed-base buildings (NRI group)

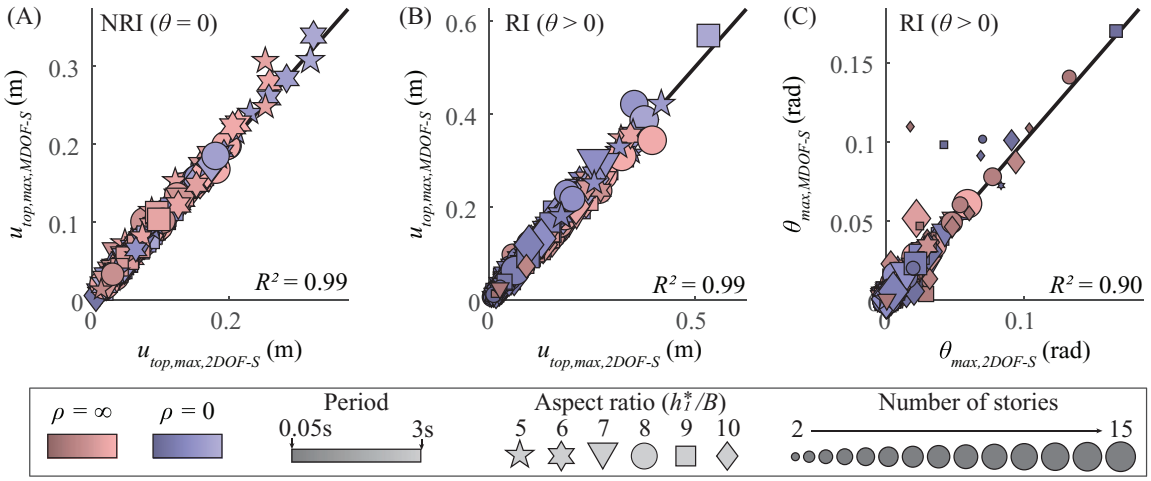

FIGURE 9 Comparison between MDOF-S and 2DOF-S model maximum relative top displacement $u_{top,max}$ and base rotation angle θ_{max} response quantities of interest obtained from 306 NRI (panel A) and 693 RI (panels B and C) simulation pairs featuring the same randomly generated prototype MDOF rocking structure and the same horizontal ground motion excitation. The building characteristics are shown as follows: the symbol identifies the aspect ratio, the color scale identifies the period, the color (red or blue) identifies the building behavior type ($\rho = \infty$ or $\rho = 0$, respectively), and the size of the marker identifies the number of stories. The specific ground motions used in the simulations are not identified in this figure. NRI, no rocking initiation; RI, rocking initiated.

with a high number of stories, and consequently a long period, is significantly influenced by higher-mode contributions, which are not captured by the 2DOF-S model. Additionally, the prototype MDOF rocking structures with low aspect ratios (5 and 6 in Figure 9A) displace the most in the NRI group. This is because such structures are not prone to rocking and develop large displacements while their base does not uplift. More slender structures do displace more, but they are easier to uplift and, thus, belong to the RI group.

The RI group contains the remaining 693 simulations in which rocking was initiated, but the structure is re-centered at the end of the ground motion excitation. We compared the models for two response quantities of interest. The 2DOF-S model agrees well with the MDOF-S model for the maximum displacement of the top mass $u_{top,max}$, with the coefficient of determination $R^2 = 0.99$, as shown in Figure 9B. The phenomenon noticed previously is evident again: the 2DOF-S model of shear- and flexure-dominant structures systematically over- and under-estimates the MDOF-S model relative top displacement, respectively. If we regress $u_{top,max,MDOF-S} = c_1 \cdot u_{top,max,2DOF-S}$ separating the data for shear- and flexure-dominant structures, we calculate $c_1 = 0.97$ for the shear-dominant and $c_1 = 1.03$ for the flexure-dominant structures.

Notably, the agreement between two models in the RI group of simulations for the base rotation angle θ response quantity is not as good as for $u_{top,max}$, with the coefficient of determination $R^2 = 0.90$ (Figure 9C). We also observe several strong outliers. The strong disagreement between 2DOF-S and MDOF-S can be attributed to the high nonlinearity of the rocking equation of motion and the high dependence of the outcome on the initial conditions (i.e., the displacements and the velocities of the model masses when rocking starts). Interestingly, the outliers in Figure 9C are the structures with high aspect ratios, few stories, and low fundamental vibration periods.

3.4 | Influence of higher vibration modes

The accuracy of a surrogate model built upon modal analysis depends on the extent of the contributions of higher vibration modes to the response quantities of interest of the prototype MDOF flexible rocking structure. To start, we assume that the MDOF-S model is accurate enough to represent the response of the prototype MDOF rocking structure, that is, assuming displacement and rotations are small, neglecting the Centrifugal and Coriolis forces, simplifying the impact model, and assuming the structure does not slide do not diminish the ability of the MDOF-S model to represent the MDOF rocking structure response to horizontal ground motion excitation.

The contribution of higher vibration modes to the OV base moment of a fixed-base prototype MDOF rocking structure dictates how well a few-DOF surrogate model can predict the initiation of rocking. Since the rocking response is very sensitive to the initial conditions, predicting the initiation of rocking significantly affects the prediction of the base rotation

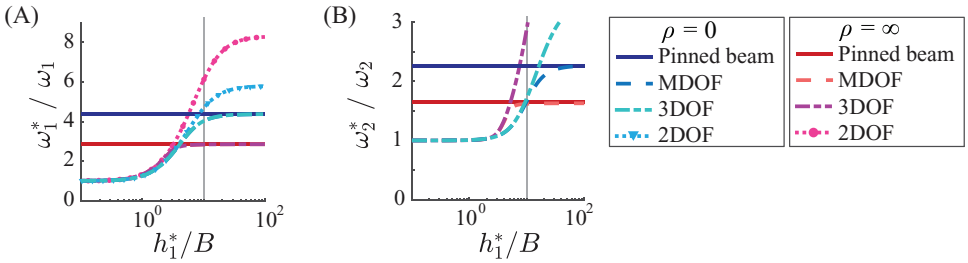

FIGURE 10 Comparisons of the MDOF-S, 2DOF-S, 3DOF-S and pinned beam[53] models of shear- and flexure-dominant 15-DOF rocking and fixed-base structures. The ratio between the first- and second-mode uplifted and fixed-base vibration frequencies are shown in (panels A and B), respectively. The gray lines indicate when $h_1^*/B = 10$.

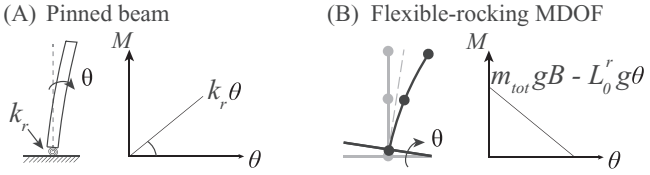

FIGURE 11 Comparison of the base moment-rotation M-θ relationships of the pinned beam, in panel A, and the MDOF flexible rocking structure, in panel B.

angle. This, in turn, affects the predictions of the base shear and the relative top displacement of the rocking structure. Therefore, to assess the influence of higher vibration modes, we analyze the response of the prototype MDOF rocking structure and its models in two situations: fixed-base and uplifted.

The influence of higher vibration modes on the response of a prototype MDOF flexible rocking structure that does not uplift is the same as that for a fixed-base MDOF structure. This problem has been thoroughly studied.[30,52] Two parameters of the MDOF structure are often used to quantify the influence of higher vibration modes on its dynamic response:[30,52,53] the modal contribution factors (e.g., $m_n^*/m_{s,tot}$, in which $m_{s,tot} = \sum_{i=1}^{N} m_i$, and $m_n^* h_n^*/L_0^r$) and the earthquake spectrum ordinate for the period of each mode (e.g., $S_a(T_n)$). This influence varies with the response quantity of interest: higher modes have a smaller effect on displacements than on forces, less effect on the base OV moment than on base shear, and they are more significant for story-level response quantities in the upper portion of the structure. Higher-mode effects also tend to gain importance as the first-mode vibration period elongates, as well as for structures whose response is dominated by flexure rather than shear. Therefore, if the prototype MDOF rocking structure behaves predominantly in flexure, is tall, and has a long first-mode vibration period, one should use the 2DOF surrogate model with care or adopt a surrogate model with a few more DOFs by specializing the MDOF-S model. We will demonstrate the 3DOF-S surrogate model later in Section 4.1.1.

The effects of higher modes on the response of a prototype MDOF flexible rocking structure that uplift and rock in response to ground motion excitation has also been investigated.[13,25,29,53,54] Uplift and subsequent rocking affects the first vibration mode of the MDOF rocking structure much more than its higher modes. Consequently, rocking (as well as the formation of a plastic hinge at the base of a fixed-base structure) does not help mitigate higher-mode effects on the response of a MDOF structure. Hence, if the higher-mode responses are important for the fixed-base MDOF structure, they will also be important if the same MDOF structure rocks.

To analyze the modal properties of the MDOF-S and 2DOF-S models in their uplifted state, we solve the frequency equations using the formulation in Silva and Stojadinović[55] (Equations 25– 28 therein). The aspect ratio of the prototype MDOF rocking structure is important for the uplifted frequencies, as the solution of the frequency equation depends on the so-called rocking frequency $p = \sqrt{(-L_0^r g)/I_\theta}$, which is a function of the structure geometry. In Figure 10, we plot the ratio between the uplifted frequencies and fixed-base first- ω_1^*/ω_1 and second-mode ω_2^*/ω_2 vibration frequencies, respectively, for two 15-story MDOF building structures, one shear-dominant $\rho = \infty$ and the other flexure-dominant $\rho = 0$. We compare the 15-mode MDOF-S model with 2DOF-S and 3DOF-S models. We also refer to the Wiebe and Christopoulous[53] pinned beam formulation that uses a beam with continuous mass and stiffness distributions. The moment-rotation behaviors of the pinned beam model and rocking MDOF-S models, shown in Figure 11, are different. The pinned beam model

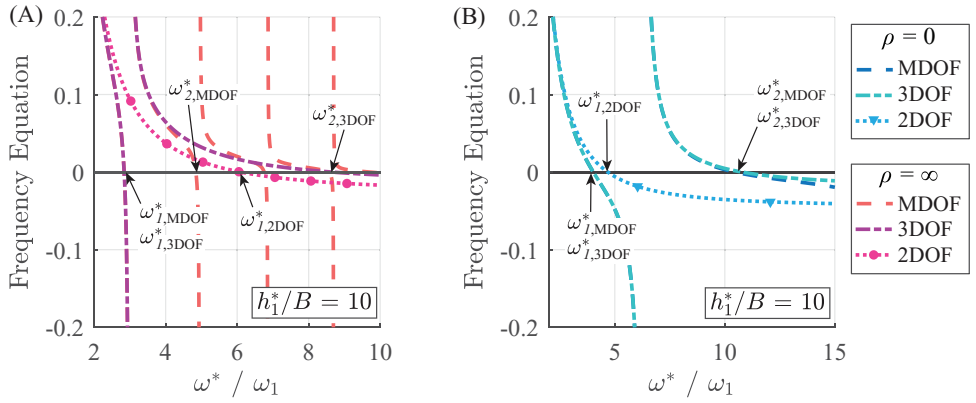

FIGURE 12 Panels A and B illustrate the solution (zero-crossing) of the frequency equations for the 2DOF-S, 3DOF-S, and MDOF-S models of the prototype 15-DOF rocking structure with aspect ratio $h_1^*/B = 10$.

has a rotational spring at its base, whose resisting moment is $M = k_r\theta$, where k_r is the positive rotational spring stiffness. The resisting moment of the rocking models is $M = m_{tot}gB - L_0^r g\theta$, which presents a negative rotational stiffness. Note that the pinned beam model whose spring rotational stiffness tends to zero ($k_r \to 0$) becomes analogous to the model of a flexible rocking column with an infinite aspect ratio ($h_1^*/B \to \infty$). Thus, the first- and second-mode vibration frequencies of the pinned beam shear- and flexure-dominant model are upper bounds of the respective frequencies of the MODF-S, 2DOF-S, and 3DOF-S models.

Analyzing Figure 10A,B, we observe that uplifted and fixed-base first- and second-mode frequencies are similar (i.e., their ratio is approximately equal to 1) for structures with lower aspect ratios, and that all models predict them well. The ability of the few-DOF surrogate models to predict the first- and second-mode frequency ratios degrades with the increasing aspect ratio of the structure.

To investigate this matter further, we plot the zero-crossing solution process of the frequency equations for the MODF-S, 2DOF-S, and 3DOF-S models of the prototype 15-DOF rocking shear- and flexure-dominant structures with an aspect ratio $h_1^*/B = 10$ in Figure 12A,B, respectively. The 2DOF-S model frequency equation solution $\omega^*_{1,2DOF}$ for the shear-dominant structure (Figure 12A) is poor. While the 3DOF-S model first-mode frequency equation solution $\omega^*_{1,3DOF}$ is quite close to the MDOF-S model solution, the second-mode frequency solution is quite inaccurate. The situation is different for the flexure-dominant structure, where the 3DOF-S and MDOF-S model frequency equation solutions for the first and the second vibration mode frequencies are essentially the same, while the 2DOF-S model first-mode frequency solution is quite good. These observations are reflected in Figure 10A,B. We conclude that the number of DOFs included in the surrogate model to estimate the first- and second-mode vibration frequencies of a 15-DOF prototype MDOF rocking structure with reasonable accuracy depends on the aspect ratio of the structure and its predominant behavior. A 2DOF-S surrogate model is likely satisfactory for flexure-dominant structures with aspect ratios smaller than 10 and shear-dominant structures with aspect ratios smaller than 5.

Lastly, we investigate if it is possible to apply a modal combination rule to account for higher modes responses, as proposed by Yim and Chopra.[25] Specifically, we use the SRSS modal combination rule to combine the maximum response estimate obtained using a 2DOF-S model of the prototype MDOF rocking structure with the maximum response estimate response obtained using a fixed-base SDOF model whose frequency ω_2 is the second vibration mode frequency of the fixed-base prototype MDOF structure (both models have the same viscous damping ratio). First, we investigate the ability of the fixed-base second-mode SDOF model to estimate the maximum displacement attained by the second vibration mode of the MDOF-S model. To do this, we plot the second mode coordinate's displacement $D_{2,max}$ of Equation (23) versus the spectral displacement $S_d(\omega_2)$ of a SDOF system with frequency ω_2 for the same earthquake ground motion and the same damping ratio for the 693 simulation pairs in the RI group. As shown in Figure 13A, the fixed-base second-mode SDOF system underestimates the second-mode displacement of the rocking MDOF-S model. Then, we compare the estimates of the maximum relative top displacement $u_{top,max}$ (Figure 13B), maximum normalized base shear $V_{b,max}/(m_{s,tot}g)$ (Figure 13C) and maximum normalized base OV moment $M_{b,max}/(L_0^r g)$ (Figure 13D) obtained using the MDOF-S model, to the one calculated using an SRSS modal combination of the 2DOF-S model estimate and the second-mode fixed-base SDOF estimate, that are: $\hat{u}_{top} = \sqrt{u^2_{top,2DOF-S} + (\Gamma_2\,\phi_{top,2}\,S_d(\omega_2))^2}$, $\hat{V}_b =$

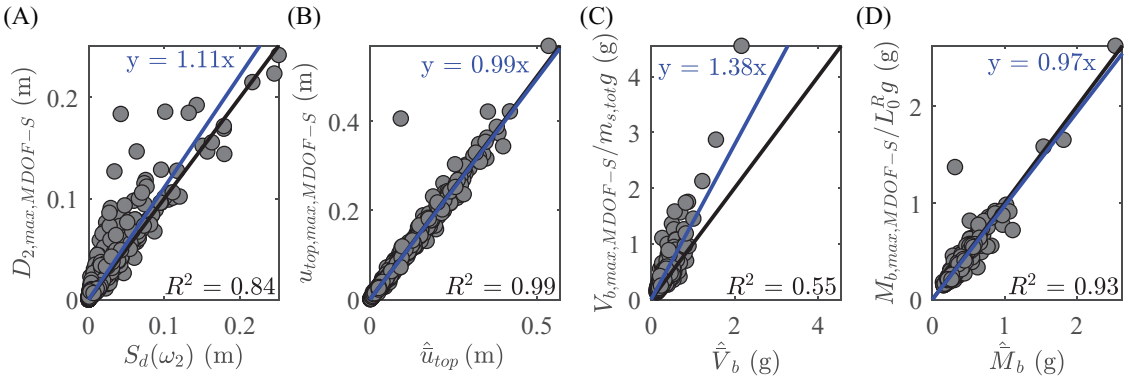

FIGURE 13 (Panel A) shows a comparison between the maximum absolute displacement of the second mode coordinate $D_{2,max}$ (Equation 23) to the maximum displacement of the second-mode fixed-base SDOF system induced by the same earthquake ground motion $S_d(\omega_2)$. (Panels B, C, and D) show comparisons of maximum relative top displacement, base shear and base OV moments obtained using the MDOF-S model and SRSS modal combination of the maximum responses of the 2DOF-S model and a second-mode fixed-base SDOF model. OV, overturning; SRSS, square root of the sum of the squares.

$\sqrt{V_{b,2DOF-S}^2 + (m_2^* S_a(\omega_2))^2}/m_{s,tot}g$ and $\hat{M}_b = \sqrt{M_{b,2DOF-S}^2 + (m_2^* h_2^* S_a(\omega_2))^2}/L_0^R g$. Furthermore, we compare those two previous results with the ones obtained using only the 2DOF-S model estimate; however, these results are not shown in Figure 13 for clarity. Also, we regress the data to analyze systematic trends: these results are shown using blue lines in Figure 13 and their respective regression equations. The SRSS modal combination delivered very good estimates of the maximum relative top displacement ($R^2 = 0.99$ and no systematic trend, with only one outlier, Figure 13B) and good estimates of the maximum base OV moment ($R^2 = 0.93$, with slight overestimation, Figure 13D), while the maximum base shear was generally underestimated and not very precise ($R^2 = 0.55$, Figure 13C). It is important to note that the modal combination significantly improved the maximum base shear estimate obtained using the 2DOF-S model alone ($R^2 = 0.41$), while for maximum base OV moment ($R^2 = 0.93$) and for maximum relative top displacement ($R^2 = 0.99$) it made almost no difference (the 2DOF-S model alone is slightly worse). Therefore, in general, the modal combination rule proposed by Yim and Chopra[25] works and can be used for structures in the same range of input parameters as the ones analyzed herein (see Figure 8).

4 | APPLICATIONS OF THE MDOF ROCKING STRUCTURE SURROGATE MODELS

In the previous section, we compared the abilities of different models to represent the relevant seismic response quantities of a prototype MDOF flexible rocking structure. We found that the 2DOF-S surrogate model, derived by considering only the fundamental vibration mode of the MDOF structure above the base that can uplift and rock, is sufficiently accurate within the parameter space we investigated to be used in design practice. In this section, we present the range of possible uses of the 2DOF-S surrogate model. First, we examine the structures whose response above the base is expected to be elastic and demonstrate how to extend the 2DOF-S model, or specialize the MDOF-S model, to include the effects of one or more higher vibration modes. Then, we extend the 2DOF-S model to simulate the inelastic response of the structure above its base.

4.1 | Elastic prototype MDOF rocking structure

The 2DOF-S surrogate model of a prototype MDOF rocking structure has eight parameters: m_1^*, h_1^*, ω_1, Γ_1, I_θ, L_0^r, M_r, and ζ. Four of the eight parameters depend on the mode shape of the MDOF structure used to develop the model, three depend on the geometry and the mass distribution of the structure, and the last parameter is the damping ratio. The formulae for the eight parameters are presented in Table 2.

The 2DOF-S model is well suited for practical applications if the elastic response of the fixed-base prototype MDOF structure above its base can be estimated using the modal analysis approach with sufficient accuracy, that is, structures that

TABLE 2 Formulae of the eight 2DOF-S surrogate model parameters.

Parameter	m_1^*	h_1^*	ω_1	Γ_1	I_θ	L_0^r	M_r	ζ
Formulae	$\frac{(\sum m_i\phi_{i,1})^2}{\sum m_i\phi_{i,1}^2}$	$\frac{\sum m_i h_i\phi_{i,1}}{\sum m_i\phi_{i,1}}$	$\sqrt{\frac{\phi_1 \boldsymbol{k}_s \phi_1}{\phi_1 \boldsymbol{m}_s \phi_1}}$	$\frac{\sum m_i\phi_{i,1}}{\sum m_i\phi_{i,1}^2}$	$\sum m_i(B^2+h_i^2)$	$\sum m_i h_i$	$\sum m_i g B$	ζ

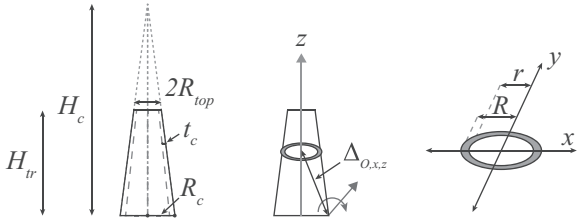

FIGURE 14 Reinforced concrete chimney geometry and the variables used to calculate the rotational inertia of the chimney.

are reasonably regular in plan and elevation. In addition, the prototype MDOF structure and its base must be symmetric with respect to one or more vertical axes, so as to have the same geometric and mass properties for any rocking pivot point.

Regular multistory building structures are often represented using simplified structural models. Equivalent frame models are exemplified by a single-bay uniform story mass and stiffness frame,[30] or a single-column multiple-beam "fish-bone" model.[56] Equivalent wall models are exemplified by a coupled cantilever beam model with varying shear-to-flexure participation ratio.[57] Obtaining the eight 2DOF-S surrogate model parameters listed in Table 2 using any of these models is straightforward. After assuming a behavior mode (flexure, shear or a combination specified by ρ for an equivalent frame model) and a distribution of the total mass m_{tot} and stiffness along the height H, the fundamental vibration mode shape ϕ_1 and vibration frequency ω_1 can be computed. Thereafter, it is straightforward to calculate the values of Γ_1, m_1^*/m_{tot}, and h_1^*/H. The rocking base moment-rotation relation parameters I_θ, L_0^r, and M_r also depend on the geometry of the structure. Modern low-damage structures often feature a rocking base restrained by a tendon.[58] The tendon exerts additional compression, thereby delaying uplift and enhancing restitution of the structure. This effect can be represented by modifying the uplift-resisting moment M_r at the base of the structure. In addition, the effect of the tendon on the elastic properties of the MDOF structure, if any, can be represented by modifying its fundamental vibration mode shape.

4.1.1 | Application example: Reinforced concrete chimney

We chose a truncated circular cone concrete chimney to show that few-DOF surrogate models can be used to model the responses of a prototype flexible rocking structure with mass and stiffness continuously distributed along its height. Due to its size, the seismic performance of the chimney may benefit from allowing its base to uplift and rock; however, its vibration properties are not straightforward to calculate. Moreover, as the chimney is tall and flexible, the effect of higher modes on its seismic response may be significant. Therefore, we also use this example to demonstrate how to extend the 2DOF-S surrogate model using higher vibration mode shapes.

The properties of the chimney are described in Exercise 8.7 of Chopra,[30] and are restated herein for completeness. It has a height $H_{tr} = 200\,m$, a circular ring cross-section whose radius varies linearly from $R_c = 8\,m$ at the base to $R_{top} = 4\,m$ at the top, and a $t_c = 1\,m$ thick wall (Figure 14). The reinforced concrete density is $\rho_c = 2400\,kg/m^3$, and the modulus of elasticity is $E_c = 25\,GPa$. The external radius of the chimney cross-section at height z above its base is $R(z) = (H_c - z)R_c/H_c$, resulting the distributed moment of inertia of the chimney ring section $I(z) = \pi(R(z)^4 - (R(z) - t_c)^4)/4$ and the distributed mass $m(z) = \rho_c\pi(R(z)^2 - (R(z) - t_c)^2)dz$.

We start by calculating the 2DOF-S model parameter I_θ (Table 2). The rotational inertia of a hollow disk rotating about a horizontal axis at the pivot point is $I = m((R^2 + r^2)/4 + \Delta_{O,x,z}^2)$ (Figure 14). Thus:

$$I_\theta = \int_0^{H_{tr}} \left(\frac{\left(\frac{(H_c - z)R_c}{H_c}\right)^2 + \left(\frac{(H_c - z)R_c}{H_c} - t_c\right)^2}{4} + z^2 + R_c^2 \right)$$

TABLE 3 Modal properties of the reinforced concrete truncated cone chimney calculated using the Rayleigh-Ritz method.

Mode	ω_n (rad/s)	m_n^* (10^6 kg)	h_n^* (m)	Γ_n
1	1.66	8.48	141.63	1.73
2	7.76	3.32	51.33	−1.19
3	19.94	1.39	31.40	0.81
4	38.14	0.75	22.51	−0.60
5	62.74	0.52	17.25	0.47

$$\rho_c\pi\left(\left(\frac{(H_c-z)R_c}{H_c}\right)^2-\left(\frac{(H_c-z)R_c}{H_c}-t_c\right)^2\right)dz=24'178'750\pi\rho_c\,. \tag{33}$$

We use the same rationale to calculate L_0^r:

$$L_0^r=\int_0^{H_{tr}} z\rho_c\pi\left(\left(\frac{(H_c-z)R_c}{H_c}\right)^2-\left(\frac{(H_c-z)R_c}{H_c}-t_c\right)^2\right)dz=\frac{580000\pi\rho_c}{3}\,, \tag{34}$$

and the resisting moment:

$$M_r=g\int_0^{H_{tr}} R_c\rho_c\pi\left(\left(\frac{(H_c-z)R_c}{H_c}\right)^2-\left(\frac{(H_c-z)R_c}{H_c}-t_c\right)^2\right)dz=17'600\pi\rho_c g\,. \tag{35}$$

We use two different methods to calculate the remaining surrogate model properties (Table 2): the finite element method and the Rayleigh-Ritz method (Chapter 18 in Chopra[30]). With the finite element method, we build the mass matrix $\boldsymbol{m_s}$ and stiffness matrix $\boldsymbol{k_s}$ of the chimney using 2000 elastic beam-column finite elements distributed continuously along the vertical axis of the chimney. We assign a mass and stiffness to each element according to its location along the height. Then, we perform a modal analysis of these matrices to obtain the chimney vibration mode shapes and parameters $m_1^*=8.485\times10^6\,kg$, $h_1^*=141.66\,m$, $\omega_1=1.678\,rad/s$, and $\Gamma_1=1.725$. Given that the modal participation factors: $m_1^*/m_{tot}=0.51$ and $m_1^*h_1^*/L_0^r=0.82$ indicate the base shear V_b and the base moment M_b may not be computed accurately enough using the fundamental vibration mode shape, we extend the 2DOF-S surrogate model using the MDOF-S surrogate model formulation (Equations 23–25) with the first two fundamental modes of vibration, to obtain a 3DOF-S surrogate model. We calculate the additional parameters: $m_2^*=3.233\times10^6 kg$, $h_2^*=50.02\,m$, $\omega_2=7.75\,rad/s$ and $\Gamma_2=-1.179$. Then, $(m_1^*+m_2^*)/m_{tot}=0.71$ and $(m_1^*h_1^*+m_2^*h_2^*)/L_0^r=0.94$, indicating that the 3DOF-S model can be used to more accurately estimate the base shear and base moment of the chimney. The process of extending the 2DOF-S model by adding higher vibration modes of the chimney can continue until sufficient accuracy is attained for all response quantities of interest.

To estimate the vibration mode shapes of the chimney using the Rayleigh-Ritz method, we adopt the following shape functions to start the process:

$$\hat{\phi}_n(z)=1-\cos\left(\frac{(1+(n-1)\cdot2)\pi z}{2H_{tr}}\right), \tag{36}$$

for modes $n=1$ to $n=5$. After two iterations, we obtain the properties of the five modes listed in Table 3.

Using the computed model parameters and Equations (23)–(25), we formulate three chimney surrogate models with a rocking base: 2DOF-S, 3DOF-S, and 6DOF-S. For comparison, we also formulate a fixed-base 5DOF model (5DOF-Fix). We use the North-South horizontal component of the El Centro record of the 1940 Imperial Valley earthquake (available in Chopra),[30] scaled up by a factor of two to excite the four models and plot the time histories of the relevant response quantities in Figure 15. Allowing the chimney to uplift and rock reduced the base moment by about 44% and the base shear by about 24%. The number of uplift events remained small and the rocking angle did not exceed 3.2×10^{-3} rad, as shown in Figure 15A. Taking the 6DOF-S model as the benchmark, we find that the prediction of the maximum relative top displacement using the few-DOF surrogate models is accurate (5.8% error for the 2DOF-S and 0.6% error for the 3DOF-S model). The prediction of the base rotation is accurate by the 3DOF-S surrogate model (2.2% error), but the prediction

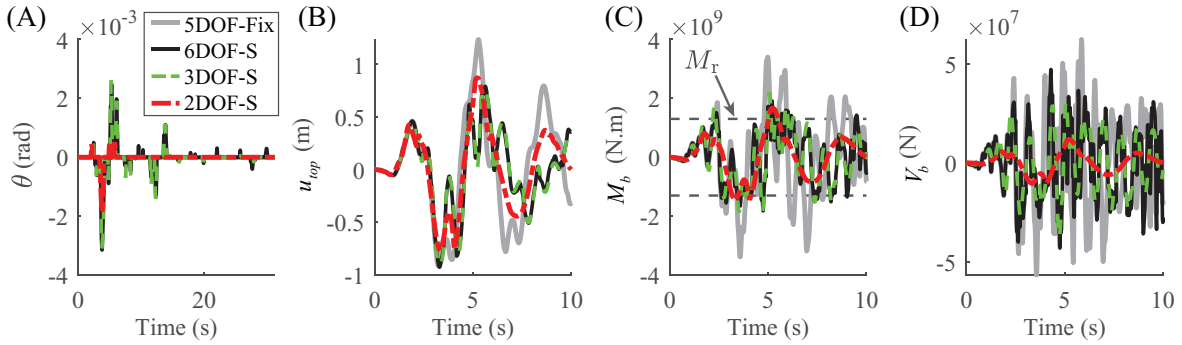

FIGURE 15 Rotation θ (panel A), relative top displacement u_{top} (panel B), base OV moment M_b (panel C), and base shear V_b (panel D) response history of the different concrete chimney models submitted to 1940 El Centro ground motion scaled up by a factor of two. The models are differentiated by color and line type: gray continuous is the fixed-base five modes MDOF model, black continuous is the rocking 6DOF-S model, green dashed is the rocking 3DOF-S model, and red dashed is the rocking 2DOF-S model. OV, overturning.

by the 2DOF-S model is not (41% error). Interestingly, the 2DOF-S model base moment prediction is more accurate, but unconservative (under-predicted by 13%), while the 3DOF-S model overestimates the base moment by 15%. Lastly, the importance of higher modes is highlighted for the chimney base shear response quantity of interest: the prediction by the 3DOF-S model is not accurate (19% error), but the prediction by the 2DOF surrogate model is unacceptable (75% of error). Extending the surrogate model to include the first three modes (i.e., a 4DOF surrogate) would further improve the estimate of the chimney base shear.

4.2 | Inelastic prototype MDOF rocking structure

We assumed that the response of the MDOF structure above its base remains elastic, and that uplift and rocking of the base are the only sources of inelastic and nonlinear behavior of the prototype structure. However, it is possible that the resistance of the MDOF structure is small enough that it yields.

We analyze the possibility of yielding of the MDOF structure and the possible interactions between rocking and yielding by including an approximate model of the inelastic behavior of the superstructure in Equation (30). The force to displacement linear relationship: $F_s(D_1) = \omega_1^2 D_1$ is replaced by a Bouc-Wen[59,60] nonlinear force-displacement hysteresis model:

$$F_{s,BW}(D_1) = \omega_1^2 \alpha_{BW} D_1 + \omega_1^2 D_{1,y}(1-\alpha_{BW})z\,, \tag{37}$$

in which α_{BW} is the post-yield stiffness, z is a yield function, and $D_{1,y}$ is the yield displacement of the oscillator of frequency ω_1. In a Bouc-Wen model, the derivative of the yield function z with respect to time is

$$\dot{z}(t, D_1) = \frac{1}{D_{1,y}}\left(\dot{D}_1 - \gamma_{BW}|\dot{D}_1|z|z|^{n_{BW}-1} - \beta_{BW}\dot{D}_1|z|^{n_{BW}}\right), \tag{38}$$

where γ_{BW}, n_{BW}, and β_{BW} are the hysteresis shape parameters. In this paper we adopt $\gamma_{BW} = 0.5$, $\beta_{BW} = 0.5$, $\alpha_{BW} = 0.01$, and $n_{BW} = 8$.

Using this Bouc-Wen formulation for a yielding oscillator, we extend the 2DOF-S surrogate model solver to obtain model 2DOF-S-BW. Then, we model a five-story shear-dominant prototype frame MDOF rocking structure with a period of 1.0 s and an aspect ratio of 10 (already used in Section 3.3) using 2DOF-S and 2DOF-S-BW surrogate models that can uplift and rock, as well as the 2DOF-S-BW model whose base is effectively fixed by assuming that it is infinitely wide ($B \to \infty$). We excite these three models with the North-South component of the 1940 Imperial Valley (El Centro) ground motion record. The time histories of the relevant response quantities are shown in Figures 16 and 17. It is noticeable from Figure 16A that rocking prevents yielding and vice-versa. To induce such behavior, the yield displacement $D_{1,y}$ was selected carefully to obtain a 2DOF-S-BW surrogate model that rocks and yields and make the comparisons. The yield displacement $D_{1,y}$ of the 2DOF-S-BW surrogate model in Figure 16 is 0.045 m. In contrast, the yield displacement $D_{1,y}$ of the 2DOF-S-BW and the

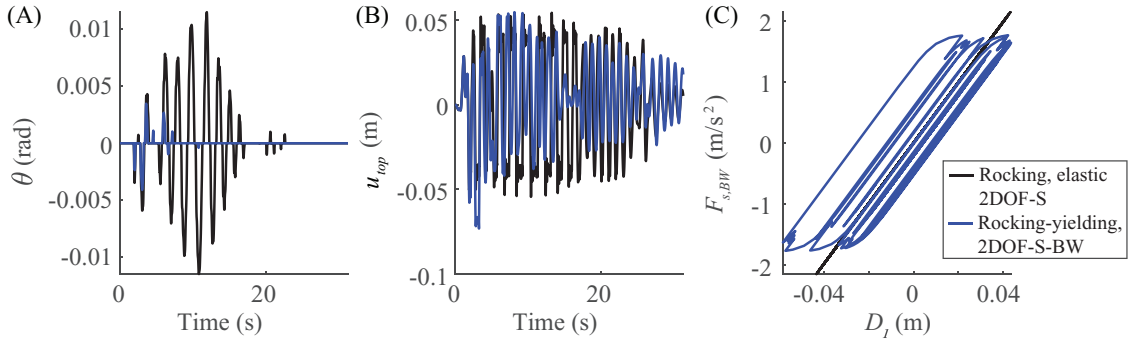

FIGURE 16 Comparison between the rotation θ (panel A), relative top displacement u_{top} (panel B) and force-displacement hysteresis (panel C) responses of a rocking elastic 2DOF-S (black continuous line) and rocking inelastic 2DOF-S-BW (blue continuous line) models subjected to the North-South horizontal component of the 1940 Imperial Valley earthquake (available in Chopra [30]).

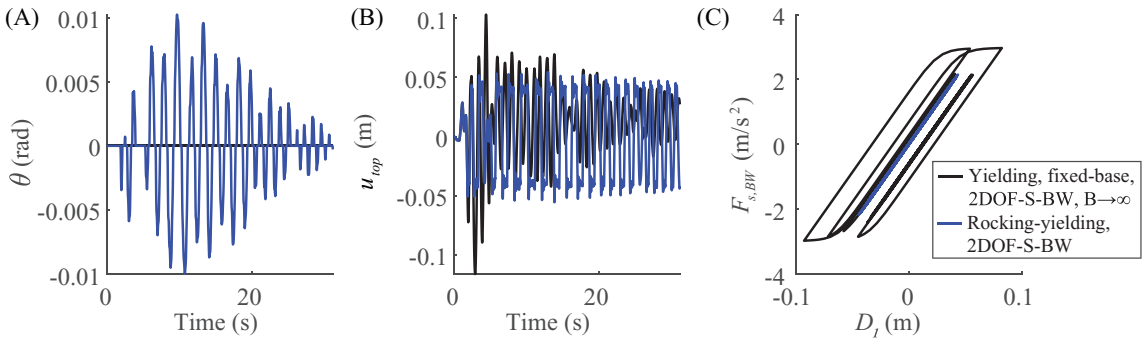

FIGURE 17 Comparison between the rotation θ (panel A), relative top displacement u_{top} (panel B) and force-displacement hysteresis (panel C) responses of a fixed-base inelastic 2DOF-S-BW (with $B \to \infty$, black continuous line) and the rocking inelastic 2DOF-S-BW (blue continuous line) models subjected to the North-South horizontal component of the 1940 Imperial Valley earthquake (available in Chopra [30]).

fixed base 2DOF-S-BW surrogate models in Figure 17 is 0.075 m. Generally, when the response of the 2DOF-S-BW model is inelastic, either rocking or yielding dominates. Namely, the 2DOF-S-BW surrogate model in Figure 17 barely yields but it clearly rocks ($\theta \approx 0.01$), while a different 2DOF-S-BW surrogate model in Figure 16 barely rocks but it clearly yields. It is also notable that the maximum relative top displacements of the two 2DOF-S-BW models are approximately the same ($u_{top} \approx 0.05$m), while the maximum displacement of the fixed-based yielding model is approximately twice as large.

Yielding of the MDOF structure violates the orthogonality of the vibration modes obtained by modal analysis of matrices $\boldsymbol{m_s}$ and $\boldsymbol{k_s}$, as the stiffness is not constant anymore. This violation creates modal coupling. Although such mode coupling is weak for typical regular fixed-base building structures, the phenomenon is still pertinent (see Chopra and Goel[61]). Furthermore, there is a change in the mode shapes when the MDOF structure base uplifts.[29] The yield point of the equivalent inelastic 2DOF-S-BW surrogate model obtained by modal pushover analysis[61] uses a fixed-base mode shape as the load pattern. Therefore, the validity of the yield point in an uplifted state should be re-established. Yet, the lower the aspect ratio, the more similar the mode shapes between fixed-base and uplifted MDOF structures are (Section 3.4). Thus, despite the challenges of adopting a Bouc-Wen model to represent an inelastic MDOF structure rocking on its base, we believe that this approximation is still useful for preliminary analysis and that it can be further refined in future studies.

5 | CONCLUSIONS

In this paper, we present a set of widely applicable surrogate models for multimass symmetric flexible rocking structures in a standardized notation. To develop the surrogate models, we derive the equations of motion of a MDOF flexible rocking structure that does not slide in modal coordinates and introduce a set of 2DOF surrogate models that accounts only for the first-mode coordinate and the rotation around the rocking pivot points. For completeness, we develop equations to

check if the flexible rocking structure can slide while rocking. To validate these surrogate models, we compare different 2DOF models to the MDOF-S model, focusing on non-OV earthquake ground motion responses. We find that:

- For Cloud Analysis of six different flexible rocking prototype building structures, the 2DOF surrogate models agree well with each other, but they over- and under-estimate the relative top displacement $u_{top,max}$ for the shear- ($\rho = \infty$) and flexure-dominant ($\rho = 0$) structure types, respectively. On the other hand, the statistics of the maximum rotation θ_{max} are estimated well by the 2DOF surrogate models.
- In a comparison of the maxima of the earthquake ground motion response of pairs of 2DOF-S and MDOF-S models using the coefficient of determination R^2 and randomly generated input parameters that define the flexible rocking prototype building structure, the 2DOF-S surrogate model is accurate accurate for regular multistory buildings subjected to different randomly selected ground motions. In this case, R^2 is equal to 0.99 and 0.90 for $u_{top,max}$ and θ_{max}, respectively.
- Comparing the modal properties of shear- and flexure-dominant flexible rocking structures, the flexible rocking structures whose fixed-base counterparts do not have a large influence of higher modes for the base OV moment response quantity of interest are well represented by the 2DOF-S surrogate model. Nevertheless, for regular buildings, especially those with predominantly shear behavior, and buildings with high aspect ratios, the 2DOF-S surrogate models fails to represent well the modal characteristics of the uplifted structure.

The presented 2DOF-S model is useful for preliminary seismic design and probabilistic response estimation of flexible rocking structures subjected to sets of earthquake ground motions because it features a small number of input parameters and is computationally efficient. We show that the 2DOF-S surrogate model is widely applicable and demonstrate how to extend it to accommodate an inelastic-flexible rocking structure. In future work, different impact models could be used in all presented surrogate models. Additionally, the capability of the simplified models to predict large rotations and displacements associated with OV should be investigated.

ACKNOWLEDGMENTS

The authors thank Prof. Vassiliou for sharing the experimental results and for his advice on rocking modeling. The authors also thank Prof. Acikgoz for sharing the experimental result. Finally, the authors appreciate the valuable feedback from the anonymous reviewers. The research presented herein is supported by the Swiss National Science Foundation (SNSF) under Grant 200021_184805 and the Swiss Federal Institute of Technology (ETH) Zurich. The authors gratefully acknowledge this funding. The methods, results, opinions, findings, and conclusions presented in this report are those of the authors and do not necessarily reflect the views of the funding agencies.

Open access funding provided by Eidgenossische Technische Hochschule Zurich.

CONFLICT OF INTEREST STATEMENT

The authors declare that there are no potential conflicts of interest.

DATA AVAILABILITY STATEMENT

The data that support the findings of this study are available from the corresponding author upon reasonable request.

REFERENCES

1. Housner GW. The behavior of inverted pendulum structures during earthquakes. *Bull Seismol Soc Am*. 1963;53(2):403-417.
2. Zhong C, Christopoulos C. Self-centering seismic-resistant structures: historical overview and state-of-the-art. *Earthq Spectra*. 2022;38(2):1321-1356.
3. Sharpe R, Skinner RI. The seismic design of an industrial chimney with rocking base. *Bull N Z Soc Earthq Eng*. 1983;16(2):98-106.
4. Beck JL, Skinner RI. The seismic response of a reinforced concrete bridge pier designed to step. *Earthq Eng Struct Dyn*. 1973;2(4):343-358.
5. Routledge P, McHaffie B, Cowan M, Palermo A. Wigram–Magdala link bridge: low-damage details for a more efficient seismic design philosophy. *Struct Eng Int*. 2020;30(2):177-184.
6. Wada A, Qu Z, Ito H, Motoyui S, Sakata H, Kasai K. Seismic retrofit using rocking walls and steel dampers. In: Improving the Seismic Performance of Existing Buildings and other Structures. 2010:1010-1021.
7. Marriott D., Pampanin S., Bull D., Palermo A.. Dynamic testing of precast, post-tensioned rocking wall systems with alternative dissipating solutions. Bulletin of the New Zealand Society for Earthquake Engineering. 2008;41(2):90103. https://doi.org/10.5459/bnzsee.41.2.90-103
8. Wiebe L, Christopoulos C. Mitigation of higher mode effects in base-rocking systems by using multiple rocking sections. *J Earthquake Eng*. 2009;13(S1):83-108.

9. Steele TC, Wiebe LD. Large-scale experimental testing and numerical modeling of floor-to-frame connections for controlled rocking steel braced frames. *J Struct Eng*. 2020;146(8):04020163.
10. Eatherton MR, Hajjar JF. Hybrid simulation testing of a self-centering rocking steel braced frame system. *Earthq Eng Struct Dyn*. 2014;43(11):1725-1742.
11. Bachmann J, Vassiliou M, Stojadinović B. Dynamics of rocking podium structures. *Earthq Eng Struct Dyn*. 2017;46(14):2499-2517.
12. Bantilas KE, Kavvadias IE, Vasiliadis LK. Seismic response of elastic multidegree of freedom oscillators placed on the top of rocking storey. *Earthq Eng Struct Dyn*. 2021;50(5):1315-1333.
13. Zhong CM, Christopoulos C. Shear-controlling rocking-isolation podium system for enhanced resilience of high-rise buildings. *Earthq Eng Struct Dyn*. 2022;51(6):1363-1382.
14. Newmark NM, Hall WJ. Earthquake Spectra and Design. Earthquake Engineering Research; 1982.
15. Ruiz-García J, Miranda E. Inelastic displacement ratios for evaluation of existing structures. *Earthq Eng Struct Dyn*. 2003;32(8):1237-1258.
16. Vamvatsikos D, Cornell CA. Direct estimation of seismic demand and capacity of multidegree-of-freedom systems through incremental dynamic analysis of single degree of freedom approximation. *J Struct Eng*. 2005;131(4):589-599.
17. Tsiavos A, Mackie KR, Vassiliou MF, Stojadinović B. Dynamics of inelastic base-isolated structures subjected to recorded ground motions. *Bull Earthq Eng*. 2017;15:1807-1830.
18. Kazantzi AK, Lachanas CG, Vamvatsikos D. Seismic response distribution expressions for on-ground rigid rocking blocks under ordinary ground motions. *Earthq Eng Struct Dyn*. 2021;50(12):3311-3331.
19. Makris N, Konstantinidis D. The rocking spectrum and the limitations of practical design methodologies. *Earthq Eng Struct Dyn*. 2003;32(2):265-289.
20. Yim CS, Chopra AK, Penzien J. Rocking response of rigid blocks to earthquakes. *Earthq Eng Struct Dyn*. 1980;8(6):565-587.
21. Psycharis IN, Jennings PC. Rocking of slender rigid bodies allowed to uplift. *Earthq Eng Struct Dyn*. 1983;11(1):57-76.
22. Zhang J, Makris N. Rocking response of free-standing blocks under cycloidal pulses. *J Eng Mech*. 2001;127(5):473-483.
23. Meek JW. Effects of foundation tipping on dynamic response. *J Struct Div*. 1975;101(7):1297-1311.
24. Psycharis IN. Dynamic behavior of rocking structures allowed to uplift. Tech. Rep. EERL 81-02. California Institute of Technology; 1982.
25. Yim SCS, Chopra AK. Simplified earthquake analysis of multistory structures with foundation uplift. *J Struct Eng*. 1985;111(12):2708-2731.
26. Chopra AK, Yim SCS. Simplified earthquake analysis of structures with foundation uplift. *J Struct Eng*. 1985;111(4):906-930.
27. Oliveto G, Calio I, Greco A. Large displacement behaviour of a structural model with foundation uplift under impulsive and earthquake excitations. *Earthq Eng Struct Dyn*. 2003;32(3):369-393.
28. Vassiliou MF, Truniger R, Stojadinović B. An analytical model of a deformable cantilever structure rocking on a rigid surface: development and verification. *Earthq Eng Struct Dyn*. 2015;44(15):2775-2794.
29. Acikgoz S, DeJong MJ. Analytical modelling of multi-mass flexible rocking structures. *Earthq Eng Struct Dyn*. 2016;45(13):2103-2122.
30. Chopra A. Dynamics of Structures: Theory and Applications to Earthquake Engineering. In: SI Units. 5th ed. Pearson; 2017.
31. Chopra AK, McKenna F. Modeling viscous damping in nonlinear response history analysis of buildings for earthquake excitation. *Earthq Eng Struct Dyn*. 2016;45(2):193-211.
32. Strutt J. Some general theorems relating to vibrations. *Proc London Math Soc*. 1871;1(1):357-368.
33. Minguzzi E. Rayleigh's dissipation function at work. *Eur J Phys*. 2015;36(3):035014.
34. Acikgoz S, DeJong MJ. The interaction of elasticity and rocking in flexible structures allowed to uplift. *EarSthq Eng Struct Dyn*. 2012;41(15):2177-2194.
35. Psycharis IN. Effect of base uplift on dynamic response of SDOF structures. *J Struct Eng*. 1991;117(3):733-754.
36. Truniger R, Vassiliou MF, Stojadinović B. An analytical model of a deformable cantilever structure rocking on a rigid surface: experimental validation. *Earthq Eng Struct Dyn*. 2015;44(15):2795-2815.
37. Giouvanidis AI, Dimitrakopoulos EG. Nonsmooth dynamic analysis of sticking impacts in rocking structures. *Bull Earthq Eng*. 2017;15:2273-2304.
38. Zhu H, Chatzis MN, Acikgoz S. A new impact model for the flexible rocking oscillator. *Earthq Eng Struct Dyn*. 2022;51(8):1819-1839.
39. Hurty WC. Dynamic analysis of structural systems using component modes. *AIAA J*. 1965;3(4):678-685.
40. Craig RR, Bampton M. Coupling of substructures for dynamic analyses. *AIAA J*. 1968;6(7):1313-1319.
41. MATLAB. Version 9.7.0 (R2019b). Natick, Massachusetts: The MathWorks Inc.; 2019.
42. Acikgoz S, Ma Q, Palermo A, DeJong MJ. Experimental identification of the dynamic characteristics of a flexible rocking structure. *J Earthq Eng*. 2016;20(8):1199-1221.
43. Jalayer F, Ebrahimian H, Miano A, Manfredi G, Sezen H. Analytical fragility assessment using unscaled ground motion records. *Earthquake Eng Struct Dyn*. 2017;46(15):2639-2663.
44. Reggiani Manzo N, Lachanas CG, Vassiliou MF, Vamvatsikos D. Uniform risk spectra for rocking structures. *Earthq Eng Struct Dyn*. 2022;51(11):2610-2626.
45. Lachanas CG, Vamvatsikos D, Dimitrakopoulos EG. Intensity measures as interfacing variables versus response proxies: the case of rigid rocking blocks. *Earthq Eng Struct Dyn*. 2023;52(6):1722-1739.
46. Bantilas KE, Kavvadias IE, Vasiliadis LK. Analytical investigation of the seismic response of elastic oscillators placed on the top of rocking storey. *Bull Earthq Eng*. 2021;19(2):1249-1270.
47. Manzo NR, Vassiliou MF. Cyclic tests of a precast restrained rocking system for sustainable and resilient seismic design of bridges. *Eng Struct*. 2022;252:113620.

48. Vassiliou MF, Cengiz C, Dietz M, et al,. Dataset from the shake table tests of a rocking podium structure. *Earthq Spectra*. 2021;37(3):2107-2125.
49. Vassiliou MF, Cengiz C, Dietz M, et al,. Dataset from the shake table tests of free-standing rocking bodies. *Earthq Spectra*. 2020;37(4):2971-2987.
50. Palermo A, Pampanin S, Marriott D. Design, modeling, and experimental response of seismic resistant bridge piers with posttensioned dissipating connections. *J Struct Eng*. 2007;133(11):1648-1661.
51. Chopra AK, Goel RK. Building period formulas for estimating seismic displacements. *Earthq Spectra*. 2000;16(2):533-536.
52. Christopoulos C, Zhong C. Towards understanding, estimating and mitigating higher-mode effects for more resilient tall buildings. *Resilient Cities Struct*. 2022;1(1):53-64.
53. Wiebe L, Christopoulos C. A cantilever beam analogy for quantifying higher mode effects in multistorey buildings. *Earthq Eng Struct Dyn*. 2015;44(11):1697-1716.
54. Zhong C, Christopoulos C. Scaled shaking table testing of higher-mode effects on the seismic response of tall and slender structures. *Earthq Eng Struct Dyn*. 2023;52(3):549-570.
55. Silva AHA, Stojadinovic B. A surrogate modeling approach for rocking-flexure interaction. *engrXiv*. 2021. doi: https://doi.org/10.31224/osf.io/y2g4f
56. Nakashima M, Ogawa K, Inoue K. Generic frame model for simulation of earthquake responses of steel moment frames. *Earthq Eng Struct Dyn*. 2002;31(3):671-692.
57. Miranda E, Taghavi S. Approximate floor acceleration demands in multistory buildings. I: formulation. *J Struct Eng*. 2005;131(2):203-211.
58. Vassiliou MF, Makris N. Dynamics of the vertically restrained rocking column. *J Eng Mech*. 2015;141(12):04015049.
59. Bouc R. Forced vibrations of mechanical systems with hysteresis. In: Proc. of the Fourth Conference on Nonlinear Oscillations. Prague; 1967.
60. Wen YK. Method for random vibration of hysteretic systems. *J Eng Mech Div*. 1976;102(2):249-263.
61. Chopra AK, Goel RK. A modal pushover analysis procedure for estimating seismic demands for buildings. *Earthq Eng Struct Dyn*. 2002;31(3):561-582.

How to cite this article: Alvares da Silva AH, Stojadinović B. Surrogate models for seismic response analysis of flexible rocking structures. *Earthquake Engng Struct Dyn*. 2024;1-25. https://doi.org/10.1002/eqe.4193